NASA Technical Memorandum 101028

Body Weight of Hypersonic Aircraft: Part 1

Mark D. Ardema, Ames Research Center, Moffett Field, California

October 1988

National Aeronautics and
Space Administration

Ames Research Center
Moffett Field, California 94035

SUMMARY

The load-bearing body weight of wing-body and all-body hypersonic aircraft is estimated for a wide variety of structural materials and geometries. Variations of weight with key design and configuration parameters are presented and discussed. Both hot and cool structure approaches are considered in isotropic, organic composite, and metal matrix composite materials; structural shells are sandwich or skin-stringer. Conformal and pillow-tank designs are investigated for the all-body shape. The results identify the most promising hypersonic aircraft body-structure-design approaches and their weight trends. Geometric definition of vehicle shapes and structural analysis methods are presented in appendices.

INTRODUCTION

A methodology for estimating body weight of hypersonic aircraft for use in the Ames hypersonic aircraft synthesis code (refs. 1-4) has been developed and incorporated into the code. This weight routine is also suitable for stand-alone use to evaluate body weight, and it is the use of this program in a study of hypersonic vehicle body weight that we report here. The purpose of the study is to provide comparative information regarding the key configurational, structural, and material issues of hypersonic aircraft.

One of the most important considerations is configuration selection. For hypersonic aircraft, an all-body configuration, which has no structure that is designed solely to produce lift, appears to be a possibility (fig. 1). From a weight standpoint, the all-body shape has both inherent advantages and disadvantages when compared with the conventional wing-body shape (fig. 2). Among the advantages are the elimination of the wing and smaller overall dimensions. Principal disadvantages are greater body surface area and noncircular structural sections. Characteristics of the two nominal configurations used in the present study are listed in tables 1 and 2; any input quantity can be varied parametrically. Complete geometric definitions of the two shapes may be found in appendix A.

Basic questions arise concerning the arrangement of the body structure of hypersonic aircraft. For example, the structure may either be exposed to the atmosphere ("hot" structure) or protected from atmospheric heating by an insulation system ("cool" structure). The fuel tank may either be separate from the body (nonintegral tankage) or combined with the body structure as one unit (integral tankage). The issues of wing-body versus all-body, hot structure versus cool structure, and nonintegral versus integral tankage, as well as selection of structural concepts and materials, are all inter-related and have a major impact on hypersonic aircraft performance.

In this paper, Part I of the body-weight study, we address some of these issues by analyzing the load-bearing body structure of four basic concepts. The cool cylindrical concept employs the wing-body configuration (circular cross-sections), with the body-shell structure in the shape of the vehicle mouldline and held to a temperature of 100°F. The hot cylindrical concept is the same except that the temperature of the structure is 1500°F. The cool pillow concept uses the all-body configuration (elliptical cross-sections); intersecting conical tanks are fitted within the vehicle mouldline and walls are used to connect the tank

nodes vertically (fig. 3). The structural temperature is held to 100°F. In the hot conformal concept, the structure is placed on the mouldline of the all-body vehicle and vertical tension ties connect top and bottom surfaces (fig. 3); the structural temperature is 1500°F. All concepts employ integral tankage, that is, the same structure is used to carry all bending, longitudinal, and pressure loads.

The weights of these four concepts are computed for a wide variety of structural geometries and materials, and comparisons are made. Parametric studies are made of the lightest weight combinations; among the parameters varied are design pressure, minimum gage, gross take-off weight, and structural material temperature. Analysis of these results identifies the most promising concepts as well as the most important factors influencing body structural weight.

Because our purpose in Part I of the study is to investigate a large number of options and parameters parametrically, simplifying assumptions have been made. For example, it has been assumed that structural concept, temperature, and materials are constant over the entire vehicle. Another restriction, just mentioned, is that only integral tankage is considered. Finally, thermal protection systems, including the heat shield required for cool structure concepts, and fuel boil-off penalties have not been included.

In Part II of the study, the most promising concepts identified in Part I will be subjected to a more thorough and complete analysis. Structural concepts and materials will be varied over the length of the vehicles depending on local temperature and load conditions and on local section geometry. The issue of integral vs. nonintegral tanks will be addressed. Thermal protection system weights and fuel boil-off penalties will be assessed and added to body weights. The result will be comprehensive, consistent, integrated weight estimates of hypersonic aircraft body structure for use in preliminary design decisions.

METHODS OF ANALYSIS

The vehicle configurations considered in this study are shown in figures 1 and 2; their nominal characteristics are listed in tables 1 and 2 and their geometrical definitions are given in appendix A. The body of the wing-body configuration consists of two power-law bodies of circular cross-section placed back-to-back. This configuration has a delta wing with aft-mounted elevons. The all-body is a wingless delta-planform body with elliptical cross-sections. The forebody has constant eccentricity and the after body fairs to a straight-line trailing edge. It has both canards and horizontal tails. These two shapes are representative of hypersonic configurations presently under consideration and are easily described mathematically.

The weight items considered in this study are listed in table 3. The shell can be composed of either a single skin with stiffeners (SSF) or a sandwich with double skins separated by a core (SAND) (fig. 4). The SSF arrangement always uses longitudinal ring-frames but the SAND concept is considered both with and without frames. Only the all-body shape uses walls and tension ties, the former with the cool pillow concept and the latter with the hot conformal concept (fig. 3). Also needed only for the all-body configuration is a spanwise beam at the vehicle trailing edge to introduce tail loads into the body structure. The nonoptimum weight accounts for "noncalculable" weight items such as fasteners, welds, cutout reinforcement, surface attachments, uniform gage requirements, and manufacturing constraints, and is a percentage of the previous five weight items.

The tank item is an estimate of the weight of bulkheads and other items necessary to convert the body structure into an integral fuel tank. Finally, because of the extreme sensitivity to volume of liquid

hydrogen fueled hypersonic vehicles, it is necessary to penalize the body weight in proportion to volume taken up by the structure to accurately measure structural efficiency. Volume lost to structure includes the volume of the core of sandwich shell structures and the volume between the conical tanks and the elliptical shell of the cool pillow concept, assumed to be nonusable.

Preliminary weight estimates of aircraft traditionally have been made using empirical methods based on the actual weights of existing aircraft. The fuselage designs of hypersonic aircraft, however, will be significantly different from those of existing aircraft. Among these differences are the requirement for containment of cryogenic fuel within the body, the high external temperatures and resulting thermal gradients, the presence of insulation systems, the possible use of noncircular structural shells, and the presence of high-pressure and longitudinal acceleration loads. These factors mean that an empirically based method of body weight estimation will not be valid.

On the other hand, finite-element methods of structural analysis, commonly used in aircraft detailed design, are not appropriate for conceptual and preliminary design, because of the large number of specific cases that need to be considered. One approach is to conduct detailed analyses at just a few locations on the vehicle and then extrapolate the results to the total design, but this can be misleading because of the great variety of structural, load, and geometric characteristics in a typical design.

The body structural weight estimation method in the Ames hypersonic synthesis code is based on a third approach, beam theory structural analysis. This results in a weight estimate that is directly driven by material properties, load conditions, and vehicle size and shape, and is not confined to an existing data base. Since the analysis is done station-by-station along the vehicle longitudinal axis, the distribution of loads and vehicle geometry is accounted for, giving an integrated weight that accounts for local conditions. Early development of the body structural weight methodology is reported in reference 5. The details of the methods currently used are found in appendices B and C. Recent use of the weights program is reported in references 6 and 7.

The analysis starts with a calculation of vehicle loads; three types of loads are considered—longitudinal acceleration, tank pressure, and bending moment. In the present study, all of these loads were assumed to occur simultaneously at maximum gross weight, although other options are available.

For longitudinal acceleration, longitudinal stress resultants caused by acceleration (nominally 2.0 g) are computed as a function of longitudinal vehicle station; these stress resultants are compressive in the vehicle forebody (ahead of the propulsion system) and tensile in the afterbody. For pressure loads, the longitudinal distribution of longitudinal and circumferential (hoop) stress resultants are computed for a given shell gage pressure (nominally 15 psig). There is an option to either use the pressure loads to reduce the compressive loads from other sources or not to do this; in either case, the pressure loads are added to the other tensile loads.

Bending moments are determined by methods described in reference 8. Longitudinal bending-moment distribution from a quasi-static pull-up maneuver (nominally 2.5 g with a safety factor of 1.5) are computed. Also available, but not used in this study, is the calculation of bending moments caused by landing and gust loads. For the wing-body, all pitch control comes from the elevons, while the all-body is trimmed for level fight with the canards and then uses the horizontal tails for maneuvering.

The bending moment distribution for the two nominal configurations are shown in figure 5. It is seen that the maximum value of M for the two configurations is about the same at 3×10^6 ft-lb. These distributions are very sensitive to configuration parameters. For example, use of a wing with lower sweep

(reduces root chord) and a horizontal tail instead of elevons (increases control load lever arm) both result in greatly increased bending loads on the wing-body vehicle.

After the net stress resultants are determined at each body station, a search is conducted at each station to determine the minimum amount of structural material required to preclude failure in the most critical condition at the most critical point on the shell circumference. Failure modes considered are tensile yield, compressive yield, local buckling, and gross buckling, which are all subjected to minimum gage restrictions. This material is then distributed uniformly around the circumference. The portion of the material at the sides of the body not required for resisting bending, acceleration, and pressure loads is assumed sufficient for resisting shear and torsion loads.

The maximum stress failure theory is used for predicting yield failures. Buckling calculations assume stiffened shells behave as wide columns and sandwich shells behave as cylinders. The frames required for the stiffened shells are sized by the Shanley criterion. This criterion is based on the premise that, to a first-order approximation, the frames act as elastic supports for the wide column.

The structural geometries considered in the study are listed in table 4. There are three concepts with Z-stiffened shells and longitudinal frames; one with structural material proportioned to give minimum weight in buckling (number 2), one with buckling efficiency compromised to give lighter weight in minimum gage (3), and one a buckling—pressure compromise (4). Similarly, there are three truss-core sandwich designs, two for minimal weight in buckling with (5) and without (6) frames, and one a buckling-minimum gage compromise (7).

The structural materials considered are shown in table 5. Included are materials ranging from those in current operational use to those that have been produced only in research laboratories. There are four isotropic metallic materials and three composites, two of the latter with metal matrices.

It is assumed that structural materials exhibit elastoplastic behavior. The value of material properties used are 70% of published minimum values at temperature to account for such unmodeled effects as fatigue, stress-corrosion, creep, thermal cycling, and thermal stresses.

Composite materials are assumed to consist of orthotropic lamina formed into quasi-isotropic (two-dimensionally isotropic) laminates. Each of the lamina is composed of filaments placed unidirectionally in a matrix material. Such a laminate gives very nearly minimum weight for typical aircraft structures. Published properties of such lamina are used if available. If not, they are computed assuming that the quasi-isotropic laminate is in a state of plane stress and that the laminate consists of an infinitely large number of unidirectional bundles of fibers at equally spaced directions. Composite material density, modulus, and yield strength are then obtained from the rule of mixtures.

RESULTS

Preliminary Screening

We begin our study by computing the body weight of the four basic concepts (cool cylindrical, hot cylindrical, cool pillow, and hot conformal) using the structural geometries of table 4 and the materials of table 5. The results are shown in tables 6-9. These results show that, generally, the wing-body vehicles have lighter body structure than all-body vehicles (the wing weight, however, must be added to the wing-

body vehicles to get a fair comparison). Also, as expected, advanced materials give lighter weights than do existing materials and cool structures are lighter than hot; of course, cool structure concepts will require more thermal protection system weight than hot ones. The circled values show the lightest weight structural geometries for each structural material.

Considering the cool cylindrical concept first (table 6), all materials except one are lighter in skin-stringer-frame construction. The exception is 6AL4V Titanium which is lighter in sandwich, because of its relatively low modulus. State-of-the-art materials (2014T6 Aluminum) give weight fractions down to about 0.051 while advanced materials (AMMC) give weight fractions down to approximately 0.027, about half that value. For the hot cylindrical concept (table 7), only four of the seven materials are available because of the structural temperature (1500°F). The established material, Rene 41, gives a prohibitively high weight, while the advanced materials have weight fractions in the 0.043-0.047 range. All materials are lightest in SSF construction.

The cool pillow concept (table 8) tends to be lightest in sandwich structure, because of the decreased rigidity of the flattened body cross-sections compared with the wing-body. The exceptions are the metal matrix composites, RSTC and AMMC, which are lighter in skin-stringer-frame. Existing materials give weight fractions down to about 0.086 (6AL4V) and advanced materials to 0.062 (AMMC). Finally, table 9 shows the weights for the hot conformal cases. Only the metal matrix composites in SSF construction are competitive for this concept.

For the parametric results to be discussed next, only configuration/structural geometry/structural material combinations with structural weight fractions below 0.08 will be considered. For the purpose of this selection a wing weight fraction of 0.02, typical for the type of vehicle being considered, is added to the weight fractions of all wing-body concepts. This 0.02 wing-weight fraction is included in all the parametric studies that follow. The concepts meeting the criterion are compared in figure 6. Most of these are in the cool cylindrical category. All SSF designs are number 3 in table 4, the Z-stiffened shell with frames, sized for buckling-minimum gage compromise, and all SAND designs are number 7, the frameless truss-core sandwich, sized for the same compromise.

Parametric Studies

Considering first the effects of variation in gage pressure (that is, pressure differential across the structural shell), figure 7 shows that, generally, the ratio of body structural weight, W, to gross take-off weight, W_{TO}, of the SAND designs is more influenced by pressure than that of the SSF designs (because a lower fraction of material is available for resisting hoop stresses in sandwich construction). Also, the three concepts with circular structural sections are less sensitive to pressure than is the hot conformal concept (reflecting the relative inefficiency of non-circular pressure vessels). The tick marks on the figure denote the nominal design pressure of 15 psi. The dashed line at 0.02 denotes the wing weight portion of the weight fraction.

It is seen that the sensitivity to pressure varies greatly between concepts. For example, the cool cylindrical GRAEPO/SSF combination is not influenced by pressure until about 25 psi (fig. 7a) while the hot conformal AMMC/SAND is almost completely pressure critical at the nominal value of 15 psi. All results on figure 7 are for no pressure stabilization. Selected calculations show that these results are little changed if pressure stabilization is employed.

Figure 8 shows the effect on body weight of changes in minimum gage. The nominal values of minimum gage are 0.01 in. for isotropic materials (6AL4V, RST), 0.02 in. for metal matrix composites (RSTC, AMMC) and 0.03 in. for organic composites (GRAEPO). The sensitivity to minimum gage also varies greatly with concept. Some concepts, for example the hot cylindrical RSTC/SAND (fig. 8b) and many of the cool pillow combinations (fig. 8c), have completely minimum gage structure at the nominal values of minimum gage. The SAND designs are more affected by changes in minimum gage than are the SSF because shell structures with two face sheets contain more material than those with one at the same gage thickness.

The sensitivities to a basic configuration parameter, gross take-off weight, are shown in figure 9. These curves all have the same basic shape. At very low values of W_{TO}, loads are low, structure tends to be sized by minimum gage, and as a consequence W/W_{TO} is high. As W_{TO} increases, W/W_{TO} decreases as the minimum gage constraint influences less and less of the structure. As W_{TO} further increases, W/W_{TO} eventually increases in conformance with the usual trend of aircraft structural weight. The result is that body structural weight fraction is minimum at some value of gross weight for each concept. The location of the minimum W/W_{TO} point, and hence the specific shape of the sensitivity curves, is highly dependent on structural material, structural geometry, and vehicle configuration.

The minimum body structural weight fraction point varies from around 200,000 lb gross take-off weight for the hot conformal concepts (fig. 9d) to apparently well beyond 1,000,000 lb for the cylindrical concepts (figs. 9a and b). At the higher gross weights, the wing-body configuration tends to have a significant body weight advantage over the all-body. Also, in many cases sandwich structure tends to become more competitive relative to skin-stringer-frame as W_{TO} increases.

There are two reasons the body weight fraction of the all-body configurations climbs faster with gross weight than does the body weight fraction of the wing-body. First, the all-body shape is structurally less efficient than the circular cross-section of the wing-body, meaning that the all-body structure becomes strength and stiffness critical at a lower gross weight. Second, the weight of the spanwise beam at the rear of the all-body grows at a faster rate than does the gross weight.

Figure 10 shows the sensitivity to the temperature of the load-bearing structural material. Only one set of curves is presented for the cylindrical concept, figure 10a, because both the hot and cool structure cases appear here. Although increasing temperature rapidly makes most materials uncompetitive, one class of materials, RST and RSTC, retain much of room temperature strength and stiffness to 1500°F and consequently they are almost as light in hot structure as in cool. One material/structural combination is lightest for all temperatures, vehicle configurations, and structural arrangements—AMMC/SSF.

Selected Concepts

Based on the parametric results, several concepts were selected for further comparison; their body structural weight breakdowns are shown in figure 11. A wing weight fraction of 0.02 has been added to the cylindrical configurations. All four basic concepts are compared with a common material and shell geometry—AMMC/SSF. This comparison shows that the cool cylindrical concept has the lightest weight, although if the volume penalty were removed from the cool pillow concept (for example if the volume between the circular lobes and the elliptical shell is usable) it would be equally light.

Three composite materials—RSTC, AMMC, and GRAEPO—are compared in SSF construction for the cool cylindrical concept. AMMC is lightest, followed by GRAEPO. Also on figure 11 is a

comparison of the same material, RST, in both SSF and SAND for the same vehicle configuration and structural temperature. The SSF structure has frames but the SAND does not and the SAND has a volume penalty but the SSF does not; the net result is about equal weight for both.

The longitudinal distributions of shell weight per unit surface area for the concepts of figure 11 are shown in figure 12. One of these concepts is buckling dominated (cool cylindrical RST/SSF), two are pressure dominated (hot cylindrical AMMC/SSF), and the other five are heavily influenced by the minimum gage constraint. One concept, cool cylindrical RSTC/SSF, is entirely minimum gage. These results are consistent with the parametric trends discussed earlier. Figure 12 also shows that minimum gages are highest for sandwich structure, relative to skin-stringer, and for composite materials, relative to isotropic. The relatively low density of the AMMC material makes it light in minimum gage, even though it is a composite.

CONCLUDING REMARKS

Part I of the hypersonic body weight study has identified several important characteristics and trends. It was found that, generally, the wing-body designs had lower load-bearing body weights than did the all-bodies; this is because the wing-body shape has efficient circular cross-sections, as opposed to elliptical, and lower surface area for the same volume. It was also found that skin-stringer-frame construction gives lighter weight than sandwich construction, especially for composite materials. This lighter weight is due to the relatively low bending loads on the vehicles (which is due, in turn, to low gross weight and density) and, in the case of composite materials, to high minimum gages. The exception is the pillow tank arrangement, which tends to be lighter in sandwich. The use of metal matrix composites makes hot structure competitive with cool.

The relative importance of design pressure and of minimum gage constraints is highly dependent on vehicle/structural/material combination. For some combinations, the nominal design pressure of 15 psi dominated the sizing of structural elements but for others it was insignificant. While minimum gage had at least some degree of impact on all designs, some designs were completely minimum gage. These results indicate that hypersonic aircraft structure should be designed with new considerations in mind. Proper selection of structural concepts and materials and careful attention to detail design should largely eliminate the effects of pressure, minimum gage, and thermal stress (the latter not considered in this study).

The body weight of hypersonic vehicles has a characteristic trend with respect to changes in gross take-off weight. Body weight is high at low gross weights (due to minimum gage effects) and high at high gross weights with a minimum body weight at some intermediate value of gross weight. The minimum weight point, however, is very different for the various concepts. Minimum body weight for all-body shapes occurs from 200,000 lb to 700,000 lb gross weight, and for wing-body shapes, it can be well over 1,000,000 lb. The implications are that the wing-body configuration becomes increasingly superior, from a structural standpoint, as gross weight increases and that selection of the best structural concept/material is highly dependent on gross take-off weight.

Varying the temperature of the structural material gave the result that the combination of advanced metal matrix composite material in skin-stringer-frame construction (AMMC/SSF) gave the lightest weight for all structural/vehicle concepts and all temperatures. Close competitors for the cool and hot cylindrical concepts (wing-body shape) were graphite expoxy and advanced isotropic titanium alloy, respectively,

both in skin-stringer-frame construction. For the all-body shape (cool pillow and hot conformal concepts), there were no close competitors to the AMMC/SSF combination.

The primary purposes of Part I of the hypersonic body weight study were to study weight trends and to identify promising concepts for further study. In Part II, we will further investigate these concepts by adding thermal protection system weight and by changing structural concept and material along the vehicle length to better match local geometric, load, and temperature conditions. We will also further investigate hot vs. cool structure and take up the question of integral vs. nonintegral tanks.

APPENDIX A

VEHICLE GEOMETRIES

Considering the wing-body configuration first, the wing loading, gross density, fineness ratio, and break-point ratio are defined as

$$\mu = W_{TO}/S_p \tag{A1}$$

$$\rho_B = W_{TO}/V_B \tag{A2}$$

$$R_{fin} = l/D \tag{A3}$$

$$R_{BR} = l_1/l \tag{A4}$$

where S_p is the wing planform area (see fig. A1). All symbols are defined in appendix D. The body mouldline is defined by two power-law bodies of revolution placed back-to-back. Integration gives the body volume, body planform area, and body surface area as

$$V_B = \frac{\pi D^2}{4}\left(\frac{l_1}{2P_1 + 1} + \frac{l_2}{2P_2 + 1}\right) \tag{A5}$$

$$S_B = D\left(\frac{l_1}{P_1 + 1} + \frac{l_2}{P_2 + 1}\right) \tag{A6}$$

$$A_B = \pi S_B \tag{A7}$$

respectively, where

$$l_1 = \left[\frac{2(2P_1 + 1)W_{TO}R_{BR}^2R_{fin}^2}{\pi\rho_B}\right]^{1/3} \tag{A8}$$

$$l_2 = l_1/R_{BR} - l_1 \tag{A9}$$

$$D = \frac{l_1}{R_{BR}R_{fin}} \tag{A10}$$

Thus, if wing shape parameters Λ and μ; body shape parameters P_1, P_2, R_{BR}, and R_{fin}; and body size parameters ρ_B and W_{TO} are all specified, the wing-body configuration is geometrically defined. The section properties of cylindrical shells are well known and will not be repeated here.

For the all-body, the geometry is somewhat more complex because the lifting surface may not be sized independently of the body. The wing loading, gross density, fatness ratio, and breakpoint ratio are defined as

$$\mu = W_{TO}/S_p \tag{A11}$$

$$\rho_B = W_{TO}/V_B \tag{A12}$$

$$R_{fat} = S_\pi/S_p \tag{A13}$$

$$R_{BR} = l_\pi/l \tag{A14}$$

where S_p is the body plan area and S_π is the cross-sectional area at the breakpoint (S_π is also the maximum cross-sectional area if $0.5 < R_{BR} < 1.0$). With the aid of figure A2, the body plan area, breakpoint cross-sectional area, volume, and body angle are computed to be

$$S_p = l^2/\tan\Lambda \tag{A15}$$

$$S_\pi = \pi l_\pi^2/\tan\Lambda \tan\beta \tag{A16}$$

$$V_B = \pi l_\pi l(l + l_\pi)/6 \tan\Lambda \tan\beta \tag{A17}$$

$$\beta = \tan^{-1}(\pi R_{BR}^2/R_{fat}) \tag{A18}$$

Inspection of equations (A11) through (A18) shows that the all-body geometry will be defined if the shape parameters Λ, R_{fat}, and R_{BR} ,and the size parameters ρ_B and W_{TO} are specified. Expressing the length in terms of these parameters gives

$$l = [6R_{BR}W_{TO} \tan\Lambda/(1 + R_{BR})R_{fat}\rho_B]^{1/3} \tag{A19}$$

so that the length of the all-body scales with $(W_{TO}/\rho_B)^{1/3}$ for constant shape, just as it does for the wing-body. The wing loading of this configuration in terms of the configuration parameters is

$$\mu = \left[\frac{W_{TO}(1 + R_{BR})^2 R_{fat}^2 \rho_B^2 \tan\Lambda}{36R_{BR}^2}\right]^{1/3} \tag{A20}$$

This relation is plotted for $\Lambda = 75°$, $R_{BR} = 0.67$, and $R_{fat} = 0.09$ in figure A3. The ellipse ratio a/b of the forebody is given by

$$a/b = \pi R_{BR}^2 \cot\Lambda/R_{fat} \tag{A21}$$

The section properties of elliptical shells will be needed for the weight analysis. If the semimajor and semiminor axes of the shell at a certain longitudinal station are a and b, respectively, then the cross-sectional area and perimeter are given by

$$A = \pi ab \tag{A22}$$

$$P = 4aE_{II} \tag{A23}$$

The moment of inertia about the y axis divided by the shell thickness is found from

$$I'_y = \frac{I_y}{t_s} = 4\int_o^a z^2\,ds$$

$$= 4\int_o^a \left(1 - \frac{y^2}{a^2}\right) b^2 \sqrt{1 + \frac{b^2y^2}{a^2(a^2 - y^2)}}\,dy$$

$$= 4ab^2\left[E_{II} - \left(\frac{2E_{II} - E_I}{3}\right) - \left(\frac{E_I - E_{II}}{3e^2}\right)\right] \tag{A24}$$

where E_I and E_{II} are the complete elliptic integrals of the first and second kind, respectively, and where

$$e = \sqrt{1 - (b/a)^2} \tag{A25}$$

is the eccentricity. The following approximate expressions for P and I'_y were found to give good agreement with equations (A23) and (A24) for the values of e of interest:

$$P = 2\pi a\sqrt{1 - (e^2/2)} \tag{A26}$$

$$I'_y = (\pi/4)ab^2[3 + (b/a)] \tag{A27}$$

For concepts employing pillow tankage, the structure is not in the shape of the vehicle configuration but consists of intersecting cones fitted within the elliptical cross section of the all-body as shown in figure A4. The number of circular sections or lobes is taken to be the nearest odd integer to

$$N_T = 2(a/b) + 1 \tag{A28}$$

This relation was determined empirically and gives minimum or near minimum weight for the configuration variations considered in this study. Referring to figure A4, the equations defining the ith lobe in terms of the i-1th are

$$e^2r_i^2 = e^2b^2 - d_i^2(1 - e^2) \tag{A29}$$

$$r_i \sin\theta_i = r_{i-1} \sin\theta \tag{A30}$$

$$d_i = d_{i-1} + r_{i-1}\cos\theta + r_i\cos\theta_i \tag{A31}$$

where equation (A29) is the condition of tangency of the circle and the ellipse. These equations are solved sequentially at each body station x beginning with the center lobe. The free parameter θ is available for weight and volume optimization as discussed in appendix B. The perimeter, cross-sectional area, and I'_y of the circular lobes at any section are given by

$$P_s = 2\left[\pi b - 2b\theta + \sum_{i=2}^{N_T'-1}(2\pi r_i - 2r_i\theta_i - 2r_i\theta) + 2\pi r_{N_T'} - 2r_{N_T'}\theta_{N_T'}\right] \tag{A32}$$

$$A = 2\left\{\frac{\pi b^2}{2} - \frac{1}{2}b^2(2\theta - \sin 2\theta) + \sum_{i=2}^{N_T'-1}\left[\pi r_i^2 - \frac{1}{2}r_i^2(2\theta_i - \sin 2\theta_i) - \frac{1}{2}r_i^2(2\theta - \sin 2\theta)\right]\right.$$
$$\left. + \pi r_{N_T'}^2 - \frac{1}{2}r_{N_T'}^2(2\theta_{N_T'} - \sin 2\theta_{N_T'})\right\} \tag{A33}$$

$$I_y' = 4\left[\frac{b^3}{2}\left(\cos\theta \sin\theta - \theta + \frac{\pi}{2}\right) + \sum_{i=2}^{N_T'-1}\frac{r_i^3}{2}(\cos\theta \sin\theta + \cos\theta_i \sin\theta_i + \pi - \theta - \theta_i)\right.$$
$$\left. + \frac{r_{n_T'}^3}{2}(\cos\theta_{N_T'} \sin\theta_{N_T'} + \pi - \theta_{N_T'})\right] \tag{A34}$$

where $N_T' = (N_T + 1)/2$. The perimeter of the vertical walls connecting the lobes is given by

$$P_W = 4 \sin\theta \sum_{i=1}^{N_T'-1} r_i \tag{A35}$$

A typical pillow tankage installation is shown in figure A4. In view of equation (A28), the fore-body will have a fixed number of lobes while the number of lobes in the afterbody will increase toward the rear of the vehicle. This increase results in an afterbody structure that is probably an impractical design for an actual vehicle but is convenient for use in a mathematical model.

APPENDIX B

WEIGHT ANALYSIS

In this appendix, weight estimating methods are developed for the load-carrying body structure. It is convenient to discuss the all-body conformal and pillow-tank concepts separately. The wing-body weight equations are obtained as a special case of the all-body conformal equations. Weight estimation relationships for integral and nonintegral tanks, for the span-wise beam used with the all-body shape, and for the nonoptimum weight are also presented. In addition, the volume taken up by the body structure is determined.

Body Structural Weight for Conformal Concepts

Considering first the elliptical shell, the stress resultants in the axial direction caused by longitudinal bending, axial acceleration, and pressure at a station x are

$$N_{xB} = \frac{Mb}{I_y} \tag{B1}$$

$$N_{xA} = \frac{N_x W_s}{P} \tag{B2}$$

$$N_{xP} = \frac{APg}{P} \tag{B3}$$

respectively. In equation (B2), W_s is the portion of vehicle weight ahead of station x if x is ahead the inlet entrance, or the portion of vehicle weight behind x if x is behind the nozzle exit. In equation (B3), Pg is the tank design pressure for integral tank concepts, whereas it is a nominal value of 2 psi for nonintegral tank concepts. The total tension stress resultant is then

$$N_x^+ = N_{xB} + N_{xP} \tag{B4}$$

if x is ahead of the nozzle exit, and

$$N_x^+ = N_{xB} + N_{xP} + N_{xA} \tag{B5}$$

if x is behind it. Similarly, the total compressive stress resultant is

$$N_x^- = N_{xB} + N_{xA} - \begin{Bmatrix} 0, \text{ if not pressure stabilized} \\ N_{xP}, \text{ if stabilized} \end{Bmatrix} \tag{B6}$$

if x is ahead of the inlet entrance, and

$$N_x^- = N_{xB} - \begin{Bmatrix} 0, \text{ if not pressure stabilized} \\ N_{xP}, \text{ if stabilized} \end{Bmatrix} \tag{B7}$$

if x is behind it. These relations are based on the premise that longitudinal acceleration and pressure always increase the magnitude of stress resultants; acceleration loads never decrease stress resultants, but pressure loads may relieve stress, if pressure stabilization is chosen as an option. The pressure stabilization option is available only for integral tankage. The stress resultant in the hoop direction is

$$N_y = bP_gK_p \tag{B8}$$

where K_p accounts for the fact that not all of the shell material (for example, the core material in sandwich designs) is available for resisting hoop stress. Expressions for the geometrical quantities I'_y, A, and P may be found in appendix A.

The equivalent isotropic thicknesses of the shell are given by

$$\bar{t}_{S_C} = N_x^-/F_{cy} \tag{B9}$$

$$\bar{t}_{S_T} = (1/F_{tu})\max(N_x^+, N_y) \tag{B10}$$

$$\bar{t}_{S_G} = K_{mg}t_{mg} \tag{B11}$$

for designs limited by compression, tension, and minimum gage, respectively. In equation (B11), t_{mg} is a specified minimum material thickness and K_{mg} is a parameter relating $\bar{t}_{S_G}$ to t_{mg} which depends on the shell geometry. A fourth thickness that must be considered is that for buckling limited designs, $\bar{t}_{S_B}$, as given by equation (C13).

At each fuselage station x, the shell must satisfy all failure criteria and meet all geometric constraints. Thus, the shell thickness is selected according to

$$\bar{t}_S = \max(\bar{t}_{S_C}, \bar{t}_{S_T}, \bar{t}_{S_G}, \bar{t}_{S_B}) \tag{B12}$$

If $\bar{t}_S = \bar{t}_{S_B}$, the structure is buckling critical and the equivalent isotropic thickness of the frames, $\bar{t}_F$, is computed from equation (C13). If $\bar{t}_S > \bar{t}_{S_B}$, the structure is not buckling critical at the optimum frame sizing and the frames are re-sized to make $\bar{t}_S = \bar{t}_{S_B}$. Specifically, a new frame spacing is computed from equation (C2) as

$$d = \frac{E\epsilon\bar{t}_s^2}{N_x^-} \tag{B13}$$

and this value is used in equation (C11) to determine $\bar{t}_F$.

Reference 5 shows that for pressures as low as 2 psig the pressure-induced bending loads at the ends of the semi-major axes of the elliptical shell result in prohibitively high weight, even for concepts that take these loads in ring-frames. Consequently, it is assumed that these loads are taken by internal vertical tension ties, for both integral and nonintegral tankage. At a fuselage station x, the equivalent isotropic thickness of the "smeared" tension ties is given by

$$\bar{t}_T = \frac{APg}{PF_{tu}} \tag{B14}$$

The total thickness of the body structure is then

$$\bar{t}_B = \bar{t}_s + \bar{t}_F + \bar{t}_T \tag{B15}$$

The shell gage thickness, if desired, may be computed from $t_g = \bar{t}_s/K_{mg}$. The "ideal" body structural weight is obtained by summation over the vehicle length

$$W_I = 2\pi \Sigma (\rho \bar{t}_{s_i} + \rho_F \bar{t}_{F_i} + \rho_F \bar{t}_{T_i})\, a_i \sqrt{1 - (e_i^2/2)}\, \Delta x_i \tag{B16}$$

where quantities subscripted i depend on x. The procedure just described simplifies to the special case of circular cross-section vehicles in an obvious way; tension ties are not needed with circular cross-sections.

We next discuss the derivation of the structural geometry parameters shown in table B1. The Z-stiffened shell will be used as an example of skin-stringer-frame construction. Using reference 9 and figure B1, the equivalent isotropic thickness of the smeared skin and stringers is

$$\bar{t}_s = t_s + \frac{2b_f t_f}{b_s} + \frac{b_w t_w}{b_s} = \left[1 + 1.6 \left(\frac{b_w}{b_s}\right)\left(\frac{t_w}{t_s}\right)\right] t_s \tag{B17}$$

Since only the skin is available for resisting pressure loads,

$$K_p = 1 + 1.6 \left(\frac{b_w}{b_s}\right)\left(\frac{t_w}{t_s}\right) \tag{B18}$$

For minimum gage designs, if $t_s > t_w$ t hen $t_w = t_{mg}$ and

$$\bar{t}_s = \left[\left(\frac{t_s}{t_w}\right) + 1.6 \left(\frac{b_w}{b_s}\right)\right] t_{mg} \tag{B19}$$

so that

$$K_{mg} = \left(\frac{t_s}{t_w}\right) + 1.6 \left(\frac{b_w}{b_s}\right) \tag{B20}$$

On the other hand, if $t_s < t_w$ then $t_s = t_{mg}$ and

$$\bar{t}_s = \left[1 + 1.6 \left(\frac{b_w}{b_s}\right)\left(\frac{t_w}{t_s}\right)\right] t_{mg} \tag{B21}$$

so that

$$K_{mg} = 1 + 1.6 \left(\frac{b_w}{b_s}\right)\left(\frac{t_w}{t_s}\right) \tag{B22}$$

Equations (B18), (B20), and (B22) show that for both pressure loading critical and minimum gage limited structure, (b_w/b_s) and (t_w/t_s) should be as small as possible (i.e. no stringers).

In practice, a typical design will be influenced by bending and pressure loads and by the minimum gage constraint, and thus a compromise is necessary. If buckling is of paramount importance, then a good choice is $(b_w/b_s) = 0.87$ and $(t_w/t_s) = 1.06$ because this gives the maximum buckling efficiency for this concept, $\varepsilon = .911$ (ref. 9). From equations (B18) and (B22),

$$K_p = K_{mg} = 1 + (1.6)(0.87)(1.06) = 2.475$$

This is concept 2 in tables 4 and B1. If pressure is a dominate loading condition, then $(b_w/b_s) = 0.6$ and $(t_w/t_s) = 0.6$ is a reasonable choice, giving $\varepsilon = .76$, $K_p = 1.576$, and $K_{mg} = 2.638$; this is concept 3. For minimum gage dominated structure, the geometry $(b_w/bs_s) = 0.58$ and $(t_w/t_s) = 0.90$ gives concept 4.

The geometry of the truss-core sandwich shell concept is shown in figure B2. The equivalent isotropic shell thickness of this concept is

$$\bar{t}_s = \left(2 + \frac{t_c}{t_f}\frac{1}{\cos\psi}\right)t_f \qquad \text{(B23)}$$

Reference 9 shows that optimum buckling efficiency is obtained for $(t_c/t_f) = 0.65$ and $\psi = 55°$. This gives $\varepsilon = 0.4423$, $K_{mg} = 4.820$, and $K_p = 3.132$, concept 6 in tables 4 and B1. To get a design that is lighter for pressure and minimum gage dominant structure, we choose a geometry that puts more material in the face sheets and less in the core; the choice $(t_c/t_f) = 1.0$ and $\psi = 45°$ gives structural concept 7. These calculations assume that the face sheets and core are the same material and are subject to the same minimum gage constraint.

The preceding analysis may be used to estimate the relative weights of elliptic and circular shells in bending. Consider an elliptical and a circular shell each of equal length and equal enclosed cross-sectional area. Let the structure of both shells be a frame-stabilized, integrally stiffened shell of the same material which is buckling critical, and suppose each shell to be loaded by the same bending moment (no pressure loading). Then, for the elliptical shell, equations (B16) and (C13) give

$$W_{I_{ellipse}} = \left(2\pi\rho a\sqrt{1 - \frac{e^2}{2}}\,\Delta x\right)$$

$$\times\left\{\frac{4}{27^{1/4}}\left(\frac{\pi C_F}{K_{F1}\varepsilon^3}\right)^{1/8}\sqrt{\frac{\bar{N}_x}{E}}\left[\sqrt{3 + \frac{b}{a}}\,(0.3719ab + 0.6281a^2)\right]^{1/4}\right\}$$

Setting $r = a = b$ in this expression gives

$$W_{I_{circle}} = (2\pi\rho r\,\Delta x)\left[\frac{4}{27^{1/4}}\left(\frac{\pi C_F}{K_{F1}\varepsilon^3}\right)^{1/8}\sqrt{\frac{\bar{N}_x}{E}}(2r^2)^{1/4}\right]$$

Using equation (B1) and setting $r = \sqrt{ab}$ the weight ratio is then

$$\frac{W_{I_{ellipse}}}{W_{I_{circle}}} = \left\{\left(\frac{a}{b}\right)^2 \left(1 - \frac{e^2}{2}\right)^2 \left[\frac{4}{3 + (b/a)}\right]^{3/2} \left(0.3719 + 0.6281\,\frac{a}{b}\right)\right\}^{1/4} \tag{B24}$$

This ratio, which is a function only of a/b, is plotted in figure B3. It is seen to be nearly linear—the elliptical shell being about twice as heavy as the circular one at a/b = 4. If the shells are constructed of truss-core sandwich, equations (B16), (B1), and (C1) result in the ratio

$$\frac{W_{I_{ellipse}}}{W_{I_{circle}}} = \left(\frac{a}{b}\right)^2 \sqrt{1 - \frac{e^2}{2}} \left\{\frac{4}{[3 + (b/a)](a/b)^{3/2}}\right\}^{3/5} \tag{B25}$$

This ratio is also plotted in figure B3 and also varies linearly with a/b but with a steeper slope. Since all-body configurations typically have a/b = 4, conformal structure elliptical cross-section concepts will be considerably heavier than circular cross-section concepts.

Body Structural Weight for Pillow Concepts

Because of the poor structural efficiency of elliptical shells, a special concept called pillow tankage is potentially attractive for all-body configurations. This concept consists of a shell composed of intersecting cones fitted within the elliptical body, as discussed in appendix A. The stress resultants in the circular lobes are computed according to formulas (B1) through (B8), except that equations (B2) and (B3) are replaced by

$$N_{x_A} = \frac{n_x W_s}{(P_s + P_w)} \tag{B26}$$

$$N_{x_P} = \frac{AP_g}{(P_s + P_w)} \tag{B27}$$

The various equivalent isotropic thicknesses of the shell are computed from equations (B9) through (B11) as before, and the shell thickness is selected from equation (B12). Any structural shell geometry listed in tables 4 and B1 can be used in pillow tankage; the buckling relations for these concepts may be determined from appendix C. Frame weights are computed from either equation (B13) or equation (C13), depending on whether or not the design is buckling critical.

The maximum stress resultants on the vertical walls connecting the pillow tank lobes are

$$N_{w_x} = \frac{AP_g}{(P_s + P_w)} \tag{B28}$$

$$N_{w_z} = P_g(b \cos\theta + r_2 \cos\theta_2) \tag{B29}$$

The equivalent isotropic thicknesses of the wall are given by

$$\bar{t}_{wT} = \frac{1}{F_{tu}} \max(N_{w_x}, N_{w_z}) \tag{B30}$$

$$\bar{t}_{wG} = K_{mg} t_{mg} \tag{B31}$$

for designs limited by tension and minimum gage, and the wall thickness is therefore

$$\bar{t}_w = \max(\bar{t}_{wT}, \bar{t}_{wG}) \tag{B32}$$

The ideal structural weight of pillow tankage vehicles is then obtained by summation over the body length

$$W_I = \Sigma[\rho P_{s_i} \bar{t}_{s_i} + \rho_F (P_{s_i} + P_{w_i}) \bar{t}_{F_i} + \rho_F P_{w_i} \bar{t}_{w_i}] \Delta x_i \tag{B33}$$

where quantities subscripted i depend on x.

The parameter θ (fig. A4) is available for vehicle performance optimization. The function $W_I(\theta)$ monotonically decreases within the range $0. < \theta < \pi/2$, and θ therefore should be as large as possible to minimize W_I. (Although it is possible for equation (A28) to restrict the range of θ, this limitation is not generally encountered.) However, as θ approaches $\pi/2$ the tank volume decreases (recall that the number of lobes, N_T, is fixed by equation (A28)) and thus the volumetric efficiency η, defined as the ratio of tank volume to body configuration volume, must be considered as well as W_I. For practical designs, $\eta(\theta)$ is a concave downward function having a local maximum for some value of θ on $0 < \theta < \pi/2$. The payload performance of a hypersonic vehicle, Φ, will be a function of both W_I and η, that is, $\Phi = (W_I, \eta)$; hence the rate of change of payload with respect to θ is

$$\frac{d\Phi}{d\theta} = \left(\frac{\partial \Phi}{\partial W_I}\right)\frac{dW_I}{d\theta} + \left(\frac{\partial \Phi}{\partial \eta}\right)\frac{d\eta}{d\theta} \tag{B34}$$

The necessary condition for maximum Φ gives to a first-order approximation

$$\left(\frac{\partial \Phi}{\partial W_I}\right)(W_{I_{opt}} - W_{I_o}) + \left(\frac{\partial \Phi}{\partial \eta}\right)(\eta_{opt} - \eta_o) = 0 \tag{B35}$$

where $\partial\Phi/\partial W_I$ and $\partial\Phi/\partial\eta$ are the sensitivities of payload to W_I at constant η and to η at constant W_I, respectively, and where W_{I_o} and η_o are nominal values. Values of the partial derivatives are determined from a sensitivity study performed with a mission analysis program. Equation (B35) is solved for the optimum values $W_{I_{opt}}$ and η_{opt} using Newton's method with θ as the independent parameter. For typical vehicle shapes and missions, this procedure gives values of θ from 50° to 60°.

Nonoptimum Body Structure Weight

Since the above analysis gives only the ideal weight, W_I, the "nonoptimum" weight (fasteners, cutouts, surface attachments, uniform gage penalties, manufacturing constraints, etc.) has yet to be determined. The method used here is explained with the aid of figure B4 which is a log-log plot of body weight as a function of a weight estimation parameter, χ, which accounts for the effects of gross weight, body dimensions and design load factor. The circles on the figure indicate actual body weights of existing aircraft. The lower line represents the equation developed in reference 10 to estimate body weight of wing-body hypersonic aircraft, and reflects improvements over time in design techniques and analysis methods.

The analysis developed in the present study was applied to the same existing aircraft and the resulting ideal weights are shown by the triangles. A two parameter regression analysis based on ideal

weight, W_I, and body surface area, A_B, was then employed to obtain the best fit with the advanced technology hypersonic aircraft line. The resulting body weights are shown by the squares, and the total weight of the body structure is $1.637W_I + 0.076A_B$ so that the weight of the nonoptimum material is

$$W_{NO} = 0.637W_I + 0.076A_B \tag{B36}$$

The correlation with existing aircraft is quite good (fig. B4) except for the aircraft at the extreme values of the weight parameter. This conclusion follows from the fact that the scatter of the square symbols about the lower curve is in the same pattern as the scatter of the circles (actual weights) about the upper curve.

Tank and Spanwise Beam Weights

To a first approximation, the weight of a pressurized fuel tank will be proportional to tank material density, tank pressure, and tank volume, and inversly proportional to tank material tensile strength. Thus, the weight of nonintegral tanks is given by:

$$W_{TK} = 14460 \frac{\rho_{TK} P_g V_{TK}}{F_{tuTK}} \tag{B37}$$

The proportionality constant has been determined from the weight of the tank described in reference 11. For this tank, $\rho_{TK} = 0.298$, $F_{tuTK} = 172{,}000$, $V_{TK} = 71{,}500$, $P_g = 15.3$, and $W_{TK} = 27{,}400$.

For integral tank concepts, the tank weight consists only of bulkheads and other items specifically necessary for containment of fuel within the body structure. Again using the tank of reference 11, as a reference point, for integral tanks

$$W_{TK} = 2406 \frac{\rho P_g V_{TK}}{F_{tu}} \tag{B38}$$

Because these formulas are based on an actual tank design, nonoptimum factors are not applied to tank weight.

Comparison of equations (B37) and (B38) shows that for the same materials and operating temperature and pressure, the nonintegral tank weight will be approximately six times the integral tank weight. This advantage for integral tankage is greatly reduced or eliminated, however, because in integral tankage concepts the tank pressure loads must be carried in the body structure, typically an inefficient pressure vessel, and also because the tank components typically must operate at higher temperatures.

The transverse bending moments associated with the large span at the rear of the all-body configuration require additional structure for this configuration. The weight of such structure is estimated by computing the weight of a spanwise beam capable of transmitting the horizontal tail loads into the body structure. The result is

$$W_{SB} = 9.822\rho L_T a_M^2 / d_T F_{cy} \tag{B39}$$

where L_T is the vertical tail normal force at the design load factor, d_T is the beam depth (taken to be the body depth at the location of the tail), and a_M is the beam span (taken to be the body span at the location

of the tail). The same nonoptimum factor that is applied to the body structure, 1.637, is included in equation (B39).

Structural Volume

The mission performance of hypersonic aircraft is sensitive to volume as well as to weight. Consequently, the volume taken up by the structure must be estimated and factored into mission performance calculations and design concept decisions. For the concepts considered here, there are two sources of lost volume due to the structure. The first is the volume between the lobes of the integral tank structure and the vehicle mouldline in the pillow tank concept (see fig. A4). At a station x, the difference between the area enclosed by the mouldline and the area enclosed by the pillow tankage is

$$A_\Delta = \pi ab - A \tag{B40}$$

where A is given by equation (A33). The volume decrement (lost volume) is then given by $V_{\Delta P} = \Sigma A_{\Delta_i} \Delta x_i$.

The second source of lost volume is the space between the face sheets of sandwich shells. From figure B2,

$$h = \frac{b_f}{2} \tan \psi \tag{B41}$$

and from reference 9,

$$b_f = 0.95 t_f \sqrt{\frac{K_x \bar{t} E}{N_x^-}} \tag{B42}$$

provided $N_x^- > 0$. Substituting $t_f = \bar{t}/K_p$ and equation (B42) into equation (B41) gives

$$h = K_{th} \sqrt{\frac{\bar{t}^3 E}{N_x^-}} \tag{B43}$$

where

$$K_{th} = 0.95 \frac{\sqrt{K_x} \tan \psi}{2K_p} \tag{B44}$$

For concept 6 in table B1, $K_x = 3.5$, $\psi = 55°$, and $K_p = 3.132$; this gives $K_{th} = 0.405$ as shown in table B1. At a station x, the cross-sectional area enclosed by the structure is $A_\Delta = Ph$ where P is the perimeter of the structural shell, given by equation (A23) or equation (A26). The volume decrement is then $V_{\Delta_S} = \Sigma A_{\Delta_i} \Delta x_i$ as before.

After the pillow tank volume decrement (if any) and the structural shell volume decrement (if any) have been added to get the total volume lost because of the structure, $V_\Delta = V_{\Delta_p} + V_{\Delta_s}$, the volumetric efficiency is determined from $\eta = 1 - V_\Delta/V_B$. The weight penalty from lost volume is then

$$W_{\Delta} = \frac{\partial \Phi / \partial \eta}{\partial \Phi / \partial W_I} (\eta - 1) \qquad \text{(B45)}$$

This "weight" should be included when comparing different structural concepts, in order to properly reflect the impact on mission performance. The partial derivatives in equation (B45) are the same as those in equation (B34) and are highly mission dependent.

APPENDIX C

BUCKLING EQUATIONS

In this appendix expressions are derived for the equivalent isotropic thickness of the shell required to preclude buckling, $\bar{t}_{S_B}$, and for the "smeared" equivalent isotropic thickness of the ring frames required to preclude general instability, $\bar{t}_F$. The expressions are derived for the elliptical shell of the all-body configuration; these expressions are then used to obtain the equations for cylindrical shells as a special case. The major assumptions are that the structural shell behaves as an Euler beam and that all structural materials behave elastically.

For the frame-less sandwich shell concept, it is assumed that the elliptical shell buckles at the load determined by the maximum compressive stress resultant $\bar{N}_x$, on the ellipse. Reference 12 indicates that a good approximation is obtained by assuming the structure to be a circular cylinder with the same radius of curvature as that of the ellipse at the point of application of $\bar{N}_x$. Since the maximum load occurs at the ends of the minor axis where the radius of curvature is a^2/b, the buckling equation is

$$\frac{\bar{N}_x}{(a^2/b)E} = \varepsilon\left[\frac{\bar{t}_{S_B}}{(a^2/b)}\right]^m$$

or, solving for $\bar{t}_{S_B}$

$$\bar{t}_{S_B} = (a^2/b)\left[\frac{\bar{N}_x}{(a^2/b)E\varepsilon}\right]^{1/m} \tag{C1}$$

This equation is based on small deflection theory, which seems reasonable for sandwich cylindrical shells, although it is known to be inaccurate for monocoque cylinders. Values of m and ε may be found, for example, in references 9 and 13-15 for many shell geometries. Table B1 gives values for structural concepts number 6 and 7 used in the present study, both of which are truss-core sandwich (see table 4). The quantities $\bar{N}_x$, a, b, r, and consequently $\bar{t}_{S_B}$, will vary with body station dimension x. For the wing-body, equation (C1) becomes

$$\bar{t}_{S_B} = r\left(\frac{\bar{N}_x}{rE\varepsilon}\right)^{1/m} \tag{C1'}$$

For the stiffened shell with frames concept, the common procedure of assuming the shell to be a wide column is adopted. The buckling equation is then (ref. 13)

$$\frac{\bar{N}_x}{dE} = \varepsilon\left(\frac{\bar{t}_{S_B}}{d}\right)^2$$

or, solving for $\bar{t}_{S_B}$

$$t_{S_B} = \sqrt{\frac{N_x d}{E\epsilon}} \tag{C2}$$

which is applicable for both the all-body and the wing-body. Values of ϵ for structural concepts 1 through 5 are given in table B1; The structural shells are simply stiffened, Z-stiffened, and truss-core sandwich. We next size the frames to prevent general instability failure.

In order to generalize the Shanley criterion (ref. 16) for frame sizing to elliptical shells, the stiffness of elliptical rings to inplane loads must be determined. If the methods and nomenclature of reference 17 are used, the redundant bending moment at the ends of the semimajor axis of an elliptical ring due to oppposing inplane point loads of magnitude L acting perpendicular to the ring at the ends of the semiminor axis is

$$M_a = -\frac{\int^s M' \, ds}{\int^s ds} - \frac{L}{2}a$$

$$= \frac{L}{2aE_{II}} \int_o^a y \sqrt{\frac{a^4 - a^2y^2 + b^2y^2}{a^2(a^2 - y^2)}} \, dy - \frac{L}{2} a$$

$$= \frac{La}{4}\left(\frac{E_{III}}{E_{II}} - 2\right) \tag{C3}$$

where the dimensional quantities are defined in figure 24 and

$$E_{III} = 1 + \frac{\log_e[(a/b)(1 + e)]}{(a/b)^2 e} \tag{C4}$$

The bending-moment distribution in the ring, therefore, is given by

$$M = \frac{La}{4}\left(\frac{E_{III}}{E_{II}} - 2\,\frac{y}{a}\right) \tag{C5}$$

To determine the deflection of the ring at the point of application of the load, the method of virtual work is used:

$$\delta = 2\int^s \frac{M(\partial M/\partial L)}{E_F I_F} \, ds$$

$$= \frac{2L}{E_F I_F} \int_o^a \left(\frac{aE_{III}}{4E_{II}} - \frac{y}{2}\right)^2 \sqrt{1 + \frac{b^2y^2}{a^2(a^2 - y^2)}} \, dy$$

$$= \frac{La^3}{E_F I_F}\left(\frac{2E_{II} - E_I}{6} + \frac{E_I - E_{II}}{6e^2} - \frac{E_{III}^2}{8E_{II}}\right) \tag{C6}$$

Since $L = K_S\delta$, the spring constant of the ring is

$$K_S = \frac{K_3 E_F I_F \left(\frac{\pi}{8} - \frac{1}{\pi}\right)}{8a^3 \left(\frac{2E_{II} - E_I}{6} + \frac{E_I - E_{II}}{6e^2} - \frac{E_{III}^2}{8E_{II}}\right)} \tag{C7}$$

the factor $(K_3/8)[(\pi/8) - (1/\pi)]$ being added to conform to reference 16.

It is of interest to compare the stiffness of an elliptical ring to that of a circular ring. For equal values of $E_F I_F$ and equal enclosed areas ($r = \sqrt{ab}$), the ratio of spring constants is

$$\frac{(K_S)_{ellipse}}{(K_S)_{circle}} = \frac{2\left(\frac{b}{a}\right)^{3/2}\left(\frac{\pi}{8} - \frac{1}{\pi}\right)}{\frac{2E_{II} - E_I}{3} + \frac{E_I - E_{II}}{3e^2} - \frac{E_{III}^2}{4E_{II}}} \tag{C8}$$

This ratio is plotted as a function of a/b in figure C1, and the relatively low spring constant of the elliptical ring at the values of a/b of interest indicates that the weight of the rings in elliptical shells will be greater than those of circular shells for the same conditions.

The equation for frame (ring) weight is next established. Generalizing the results of reference 16 to elliptical frames gives the following expression for the spring constant required of the frames

$$K_S = \frac{K_1 K_2 a E_{II} \bar{N}_x}{d} \tag{C9}$$

If the frames are "smeared" according to $A_F = \bar{t}_F d$, then combination of equations (C7) and C9) gives

$$\bar{t}_F = \sqrt{\frac{4C_F \bar{N}_x a^4 E_{II}\left(\frac{2E_{II} - E_I}{3} + \frac{E_I - E_{II}}{3e^2} - \frac{E_{III}^2}{4E_{II}}\right)}{K_{F1} d^3 E_F \left(\frac{\pi}{8} - \frac{1}{\pi}\right)}} \tag{C10}$$

where K_{F1} ($= I_F/A_F^2$) is the frame stiffness, and where the constants K_1, K_2, K_3 have been absorbed by "Shanley's constant," C_F, taken to be 0.625×10^{-4}. Calculations show that the expression

$$\bar{t}_F = \sqrt{\pi C_F \bar{N}_x / K_{F1} d^3 E_F}\,\sqrt{3 + (b/a)}\,(0.3719ab + 0.6281a^2) \tag{C11}$$

very closely approximates equation (C10) for the range of a/b of interest and equation (C11) is used in the weight analysis.

Since the frame spacing, d, is as yet unspecified, it may be chosen to minimize the shell plus frame weight. If the structure is buckling critical, the total smeared weight per unit surface area of the shell and frames is given by

$$(W/S) = \rho \bar{t}_{S_B} + \rho_F \bar{t}_F \tag{C12}$$

where $\bar{t}_{S_B}$ and $\bar{t}_F$ are given by equations (C2) and (C11). When (W/S) is minimized with respect to d,

$$\bar{t}_{S_B} = \left[\frac{\pi C_F\left(3 + \frac{b}{a}\right)}{K_{F1}\varepsilon^3 E_F E^3}\right]^{1/8}\left[\frac{3\rho_F N_x^{-2}}{\rho}(0.3719ab + 0.6281a^2)\right]^{1/4}$$

$$\bar{t}_F = \left[\frac{\pi C_F\left(3 + \frac{b}{a}\right)}{K_{F1}\varepsilon^3 E_F E^3}\right]^{1/8}\left[\frac{\rho^3 N_x^{-2}}{27\rho_F^3}(0.3719ab + 0.6281a^2)\right]^{1/4} \tag{C13}$$

where the optimum frame spacing is given by

$$d = \left[3\frac{\rho_F}{\rho}\sqrt{\frac{\pi C_F \varepsilon E}{K_{F1}E_F}}\sqrt{3 + \frac{b}{a}}(0.3719ab + 0.6281a^2)\right]^{1/2} \tag{C14}$$

The shell weight per unit surface area is three times the frame weight per unit surface area for least weight design. The total weight per unit surface area is

$$(W/S) = \frac{4}{27^{1/4}}\left[\frac{\pi C_F\left(3 + \frac{b}{a}\right)}{K_{F1}\varepsilon^3 E_F E^3}\right]^{1/8}\left[\rho_F \rho^3 N_x^{-2}(0.3719ab + 0.6281a^2)\right]^{1/4} \tag{C15}$$

Reduction of equations (C13)-(C15) to the case of a circular section gives the equations for the wing-body

$$\bar{t}_{S_B} = \left[\frac{\pi C_F}{K_{F1}\varepsilon^3 E_F E^3}\right]^{1/8}\left[\frac{6\rho_F N_x^{-2} r^2}{\rho}\right]^{1/4}$$

$$\bar{t}_F = \left[\frac{\pi C_F}{K_{F1}\varepsilon^3 E_F E^3}\right]^{1/8}\left[\frac{2\rho^3 N_x^{-2} r^2}{27\rho_F^3}\right]^{1/4} \tag{C13'}$$

$$d = \left(6r^2\frac{\rho_F}{\rho}\sqrt{\frac{\pi C_F \varepsilon E}{K_{F1}E_F}}\right)^{1/2} \tag{C14'}$$

$$(W/S) = 4\left(\frac{2}{27}\right)^{1/4}\left[\frac{\pi C_F}{K_{F1}\varepsilon^3 E_F E^3}\right]^{1/8}\left[\rho_F \rho^3 N_x^{-2} r^2\right]^{1/4} \qquad (C15')$$

For the pillow tank geometry, figure A4, the maximum load occurs where the radius of curvature is b. Therefore, for sandwich shell,

$$\bar{t}_{S_B} = b\left(\frac{N_x^-}{bE\varepsilon}\right)^{1/m} \qquad (C1'')$$

For the frame stiffened shell concepts, the bucking equations are

$$\bar{t}_{S_B} = \left[\frac{C_F b I_y'}{K_{F1}\varepsilon^3 E_F E^3}\right]^{1/8}\left[\frac{6\rho_F N_x^{-2}}{\rho}\right]^{1/4}$$

$$\bar{t}_F = \left[\frac{C_F b I_y'}{K_{F1}\varepsilon^3 E_F E^3}\right]^{1/8}\left[\frac{2\rho^3 N_x^{-2}}{27\rho_F^3}\right]^{1/4} \qquad (C13'')$$

$$d = \left(6\,\frac{\rho_F}{\rho}\sqrt{\frac{bI'_y}{\pi}}\sqrt{\frac{\pi C_F \varepsilon E}{K_{F1}E_F}}\right)^{1/2} \qquad (C14'')$$

$$(W/S) = 4\left(\frac{2}{27}\right)^{1/4}\left[\frac{C_F b I_y'}{K_{F1}\varepsilon^3 E_f E^3}\right]^{1/8}\left[\rho_F \rho^3 N_x^{-2}\right]^{1/4} \qquad (C15'')$$

where I_y' is given by equation (A34).

APPENDIX D

SYMBOLS

A	cross sectional area
A_B	body surface area
A_F	frame cross-sectional area
a	semimajor axis
a_M	maximum semimajor axis
b	semiminor axis
b_s	stiffener spacing, figure B1
b_M	maximum semiminor axis
b_w	stiffener depth, figure B1
C_F	Shanley's constant
D	maximum diameter of wing-body
d	frame spacing
d_i	defined on figure A4
d_T	body depth at vertical tail
E	Young's modulus of shell material
E_F	Young's modulus of frame material
E_I	complete elliptic integral of first kind
E_{II}	complete elliptic integral of second kind
E_{III}	defined b y equation (C4)
e	eccentricity, defined by equation (A25)
F_{cy}	compressive yield strength
F_{tu}	tensile ultimate strength

h	thickness of sandwich shell, figure B2
I_F	frame cross-section moment of inertia
I_y	moment of inertia about y axis
I_y'	I_y/t_s
K_{F1}	frame stiffness coefficient, I_F/A_F^2
K_{mg}	shell minimum gage factor; see equation (B11)
K_p	shell geometry factor for hoop stress
K_S	frame spring constant
K_{th}	sandwich thickness parameter
L_T	maximum vertical tail lift
l	body length
l_1	forebody length
l_2	afterbody length
l_π	distance to breakpoint; see figure A2
M	longitudinal bending moment
m	buckling equation exponent
N_{xA}	defined by equation (B2)
N_{xB}	defined by equation (B1)
N_{xP}	defined by equation (B3)
N_T	defined by equation (A28)
N_{wx}	axial stress resultant in wall
N_{wz}	vertical stress resultant in wall
N_x^+	tensile axial stress resultant
N_x^-	compressive axial stress resultant
N_y	hoop direction stress resultant

n_x	longitudinal acceleration
P	perimeter
Pg	internal gage pressure
P_S	perimeter of shell
P_W	perimeter of walls
P_1	exponent of power law of forebody of wing-body; see figure A1
P_2	exponent of power law of afterbody of wing-body; see figure A1
R_{BR}	breakpoint ratio, defined by equations (A4) and (A14)
R_{fat}	fatness ratio, defined by equation (A13)
R_{fin}	fineness ratio, defined by equation (A3)
r	radius of wing-body
r_i	defined in figure A4
S_P	plan area of lifting surface
S_π	breakpoint cross-sectional area of all-body
T	structural temperature
t_c	core thickness, figure B2
t_f	face sheet thickness, figure B2
t_s	skin thickness, figure B1
t_g	material gage thickness, $\bar{t}_S/K_{mg}$
t_w	stiffener thickness, figure B1
t_{mg}	material minimum gage thickness
$\bar{t}$	total equivalent isotropic thickness of shell and frames
$\bar{t}_B$	total equivalent isotropic thickness of body structure
$\bar{t}_F$	smeared equivalent isotropic thickness of frames

$\bar{t}_S$	equivalent isotropic thickness of shell
$\bar{t}_{S_B}$	shell thickness required to preclude buckling failure
$\bar{t}_{S_C}$	shell thickness required to preclude compressive failure
$\bar{t}_{S_G}$	shell thickness required to meet minimum gage constraint
$\bar{t}_{S_T}$	shell thickness required to preclude tensile failure
$\bar{t}_T$	smeared tension tie thickness
$\bar{t}_w$	smeared wall thickness
$\bar{t}_{wG}$	thickness of wall to meet minimum gage constraint
$\bar{t}_{wT}$	thickness of wall required to prevent tensile failure
V_B	body volume
V_{TK}	tank volume
V_Δ	volume lost due to structure
(W/S)	shell structural weight per unit surface area
W	body structural weight; see table 3
W_I	ideal body weight; see equations (B16) and (B33)
W_{NO}	weight of nonoptimum material
W_S	vehicle longitudinal weight distribution
W_{SB}	weight of spanwise beam
W_{TK}	weight of tank
W_{TO}	gross takeoff weight
W_Δ	weight penalty associated with volume lost due to structure
x	longitudinal body coordinate
y	transverse body coordinate
z	vertical body coordinate
β	body angle of all-body

δ	frame deflection
ϵ	shell buckling efficiency
η	volumetric efficiency of body structure
θ	intersection angle for pillow tanks
θ_i	defined in figure A4
Λ	sweep
ρ	shell structural material density
ρ_B	gross body density
ρ_F	frame structural material density
ϕ	payload performance
μ	wing loading
Σ	sum over body length
ψ	truss core angle, figure B2
χ	defined in figure B4

REFERENCES

1. Gregory, T. J.; Petersen, R. H.; and Wyss, J. A.: Performance Tradeoffs and Research Problems for Hypersonic Transports. J. Aircraft, vol. 2, no. 4, July-Aug. 1965, pp. 266-271.

2. Petersen, R. H.; Gregory, T. J.; and Smith, C. L.: Some Comparisons of Turboramjet-Powered Hypersonic Aircraft for Cruise and Boost Missions. J. Aircraft, vol, 3, no. 5, Sept.-Oct. 1966, pp. 298-405.

3. Gregory, T. J.; Ardema, M. D.; and Waters, M. H.: Hypersonic Transport Preliminary Performance Estimates for an All-Body Configuration. AIAA Paper 70-1224, 1970.

4. Bowles, J. V.: Ames Conceptual Studies Activities. Proceedings of the Second National Aerospace Plane Symposium, Applied Physics Laboratory, Laurel, Maryland, Nov. 1986.

5. Ardema, M. D.: Structural Weight Analysis of Hypersonic Aircraft. NASA TN D-6692, Mar. 1972.

6. Ardema, M. D.: Hypersonic Structural Concepts and Weight Trends. Proceedings of the Second National Aerospace Plane Symposium, Applied Physics Laboratory, Laurel, Maryland, Nov. 1986.

7. Ardema, M.; Kidwell, G.; and Bowles, J.: Update of NASA Ames Conceptual Design Activity. Proceedings of the Third National Aerospace Plane Symposium, Moffett Field, California, June 1987.

8. Ardema, M. D.: Analysis of Bending Loads of Hypersonic Aircraft. NASA TM X-2092, 1970.

9. Crawford, R. F.; and Burns, A. B.: Strength, Efficiency, and Design Data for Beryllium Structures. ASD-TR-61-692, Feb. 1962.

10. Anon.: Weight and Size Analyses of Advanced Cruise and Launch Vehicles. Final Report, NASA Contract NAS2-3025, Mar. 1966.

11. Heathman, J. H. et al.: Hydrogen Tankage Application to Manned Aerospace Systems. AFFDL-TR-68-75, 1968.

12. Hutchinson, J. W.: Buckling and Initial Postbuckling Behavior of Oval Cylindrical Shells Under Axial Compression. ASME Paper 67-APM-W, Dec. 1966.

13. Crawford, R. F.; and Burns, A. B.: Minimum Weight Potentials for Stiffened Plates and Shells. AIAA J., vol. 1, no. 4, Apr. 1963, pp. 879-886.

14. Vinson, J. R.; and Shore, S.: Minimum Weight Web Core Sandwich Panels Subjected to Uniaxial Compression. J. Aircraft, vol. 8, no. 11, Nov. 1971, pp. 843-847.

15. Vinson, J. R.: Optimum Design of Composite Hex-Cell and Square Cell Honeycomb Sandwich Panels Subjected to Uniaxial Compression. AIAA J., vol 24, no. 10, Oct. 1987, pp. 1690-1696.

16. Shanley, F. R.: Weight-Strength Analysis of Aircraft Structures. Second Edition, Dover, New York, 1960.

17. Timoshenko, S. P.; and Young, D. H.: Theory of Structures, McGraw-Hill, 1945.

TABLE 1.– BASELINE ALL-BODY CHARACTERISTICS

INPUT	
• GROSS TAKE-OFF WEIGHT	200,000 lb
• GROSS DENSITY	12 lb/ft^3
• FATNESS RATIO	0.108
• BREAKPOINT RATIO	0.70
• BODY SWEEP	78.5°
• PROPULSION WEIGHT	30,000 lb
COMPUTED	
• LENGTH	123 ft
• MAXIMUM HEIGHT	12.1 ft
• MAXIMUM WIDTH	50.2 ft
• BODY VOLUME	16,667 ft^3
• BODY PLANFORM AREA	3,093 ft^2
• BODY SURFACE AREA	6,987 ft^2

TABLE 2.– BASELINE WING-BODY CHARACTERISTICS

INPUT	
• GROSS TAKE-OFF WEIGHT	200,000 lb
• GROSS DENSITY	12 lb/ft^3
• FINENESS RATIO	10
• BREAKPOINT RATIO	0.75
• WING LOADING	90 lb/ft^2
• WING LEADING EDGE SWEEP	78.5°
• PROPULSION WEIGHT	30,000 lb
• WING WEIGHT	4,000 lb

COMPUTED	
• LENGTH	179 ft
• MAXIMUM DIAMETER	17.9 ft
• BODY VOLUME	16,667 ft^3
• WING PLANFORM AREA	2,222 ft^2
• BODY SURFACE AREA	5,435 ft^2

TABLE 3.– BODY WEIGHT ITEMS

- SHELL
- WALLS
- FRAMES
- TENSION TIES
- SPANWISE BEAM
- NON-OPTIMUM
- TANK
- VOLUME PENALTY

TABLE 4.– STRUCTURAL GEOMETRY CONCEPTS

1. SIMPLY STIFFENED SHELL, FRAMES, SIZED FOR MINIMUM WEIGHT IN BUCKLING
2. Z-STIFFENED SHELL, FRAMES, BEST BUCKLING
3. Z-STIFFENED SHELL, FRAMES, BUCKLING–MINIMUM GAGE COMPROMISE
4. Z-STIFFENED SHELL, FRAMES, BUCKLING–PRESSURE COMPROMISE
5. TRUSS-CORE SANDWICH, FRAMES, BEST BUCKLING
6. TRUSS-CORE SANDWICH, NO FRAMES, BEST BUCKLING
7. TRUSS-CORE SANDWICH, NO FRAMES, BUCKLING–MINIMUM GAGE–PRESSURE COMPROMISE

TABLE 5.– STRUCTURAL MATERIALS

2014T6	STATE-OF-THE-ART ALUMINUM ALLOY
6AL4V	STATE-OF-THE-ART TITANIUM ALLOY
RENE' 41	STATE-OF-THE-ART NICKEL ALLOY
RST	ADVANCED TITANIUM ALLOY
RSTC	ADVANCED TITANIUM MATRIX COMPOSITE
AMMC	VERY ADVANCED METAL MATRIX COMPOSITE
GRAEPO	GRAPHITE-EPOXY COMPOSITE

TABLE 6.– BODY STRUCTURAL WEIGHT FRACTION, W/W_{TO}, FOR COOL CYLINDRICAL CONCEPT

	MATERIAL	2014T6	6AL4V	RENE 41	RST	RSTC	AMMC	GRAEPO
STRUCTURAL CONCEPT	1	0.0584	0.0614	0.0847	0.0466	0.0495	0.0322	0.0354
	2	0.0565	0.0559	(0.0783)	(0.0426)	0.0491	0.0323	0.0340
	3	0.0519	0.0581	0.0794	0.0440	(0.0431)	(0.0269)	(0.0323)
	4	(0.0511)	0.0590	0.0819	0.0451	0.0517	0.0308	0.0356
	5	0.0866	0.0728	0.1084	0.0576	0.0904	0.0654	0.0612
	6	0.0698	0.0610	0.1079	0.0566	0.0991	0.0661	0.0660
	7	0.0728	(0.0554)	0.0847	0.0428	0.0693	0.0502	0.0465

TABLE 7.– BODY STRUCTURAL WEIGHT FRACTION, W/W_{TO}, FOR HOT CYLINDRICAL CONCEPT

	MATERIAL	RENE 41	RST	RSTC	AMMC
STRUCTURAL CONCEPT	1	0.1135	0.0502	0.0519	0.0554
	2	0.1074	0.0469	0.0512	0.0555
	3	(0.1034)	(0.0468)	(0.0458)	0.0449
	4	0.1045	0.0478	0.0539	(0.0429)
	5	0.1539	0.0670	0.0911	0.1000
	6	0.1295	0.0596	0.0996	0.0823
	7	0.1285	0.0537	0.0704	0.0817

TABLE 8.– BODY STRUCTURAL WEIGHT FRACTION, W/W_{TO}, FOR COOL PILLOW CONCEPT

	MATERIAL	2014T6	6AL4V	RENE 41	RST	RSTC	AMMC	GRAEPO
STRUCTURAL CONCEPT	1	0.1162	0.1539	0.2050	0.1210	0.1103	0.0651	0.0911
	2	0.1228	0.1409	0.1884	0.1114	(0.1040)	0.0636	0.0853
	3	0.1282	0.1476	0.1959	0.1159	0.1045	(0.0617)	0.0871
	4	0.1284	0.1480	0.1979	0.1168	0.1085	0.0656	0.0889
	5	0.1422	0.1652	0.2221	0.1325	0.1454	0.0998	0.1109
	6	0.0912	0.1030	0.1674	0.0962	0.1508	0.1053	0.1067
	7	(0.0889)	(0.0862)	(0.1334)	(0.0770)	0.1164	0.0804	(0.0827)

TABLE 9.– BODY STRUCTURAL WEIGHT FRACTION, W/W_{TO}, FOR HOT CONFORMAL CONCEPT

	MATERIAL	RENE 41	RST	RSTC	AMMC
STRUCTURAL CONCEPT	1	0.1945	0.0891	0.0793	0.0656
	2	(0.1775)	(0.0815)	0.0760	0.0643
	3	0.1859	0.0852	(0.0736)	(0.0607)
	4	0.1869	0.0858	0.0798	0.0621
	5	0.2092	0.0993	0.1246	0.1002
	6	0.2256	0.1058	0.1361	0.0966
	7	0.2424	0.1122	0.1027	0.0883

TABLE B1.– STRUCTURAL GEOMETRY PARAMETERS

STRUCTURAL CONCEPT	m	ϵ	K_{mg}	K_p	K_{th}
1	2	0.656	2.463	2.463	0.0
2	2	0.911	2.475	2.475	0.0
3	2	0.760	2.039	1.835	0.0
4	2	0.760	2.628	1.576	0.0
5	2	0.605	4.310	3.965	0.459
6	1.667	0.4423	4.820	3.132	0.405
7	1.667	0.3615	3.413	3.413	0.320

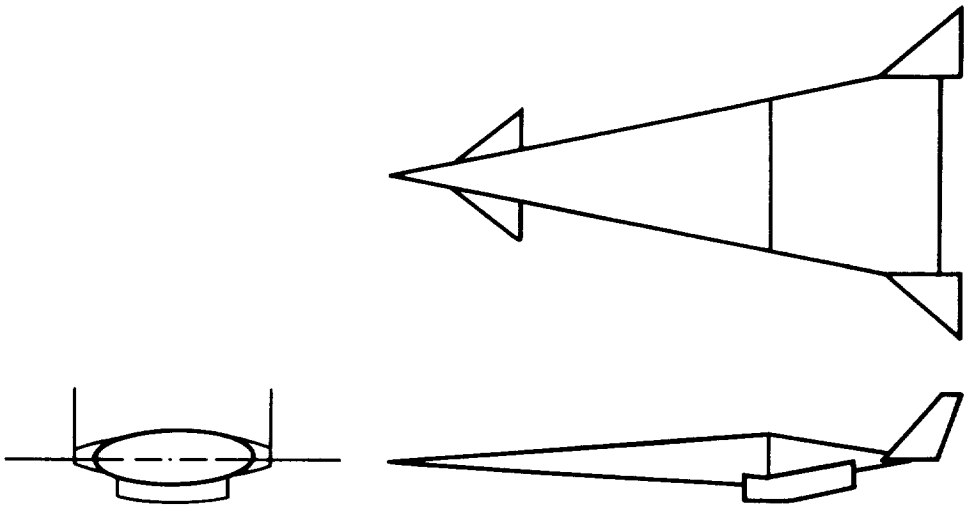

Figure 1.- The all-body configuration.

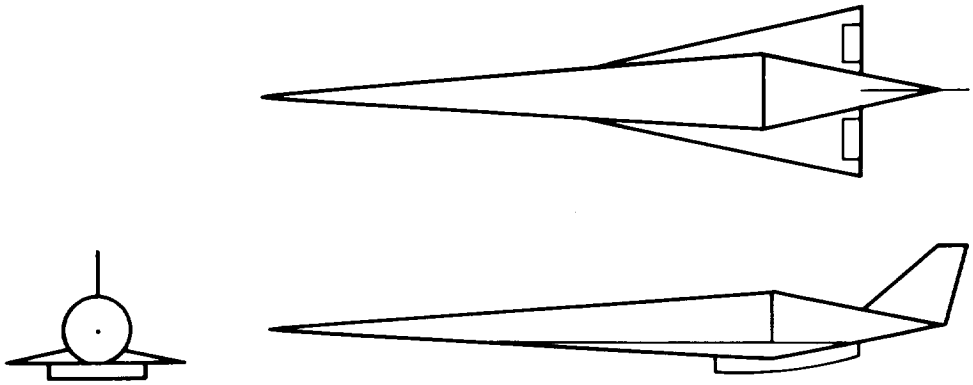

Figure 2.- The wing-body configuration.

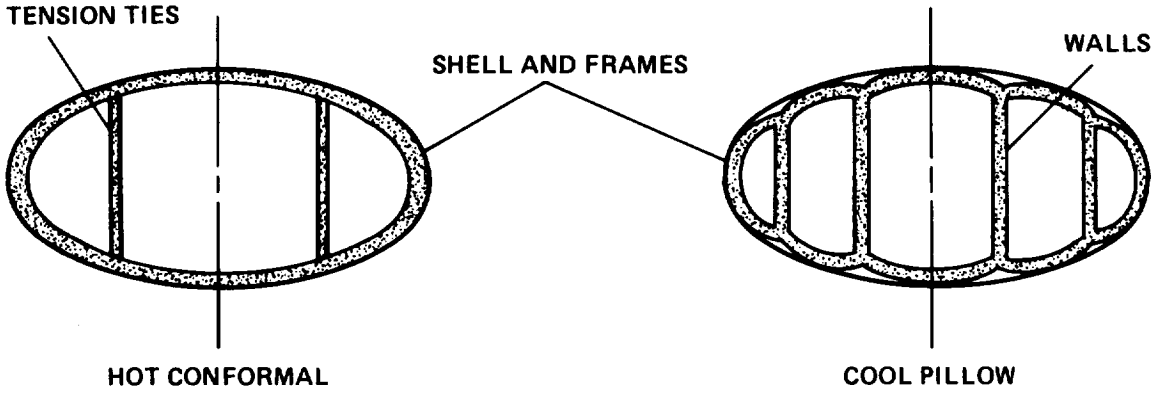

Figure 3.- All-body structural arrangements.

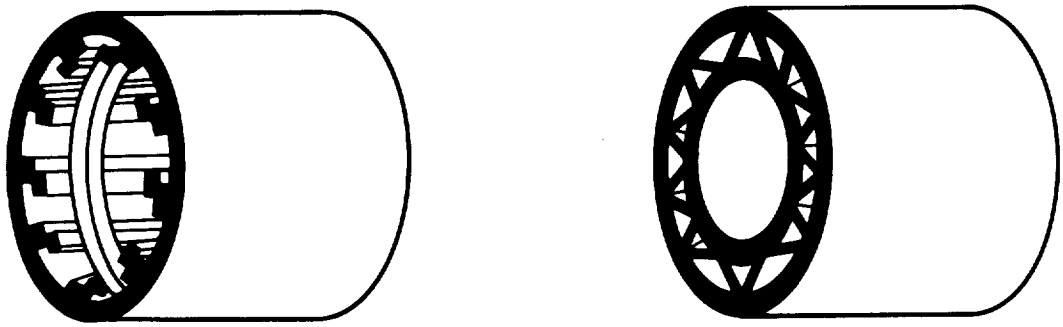

Figure 4.- Shell structural geometries.

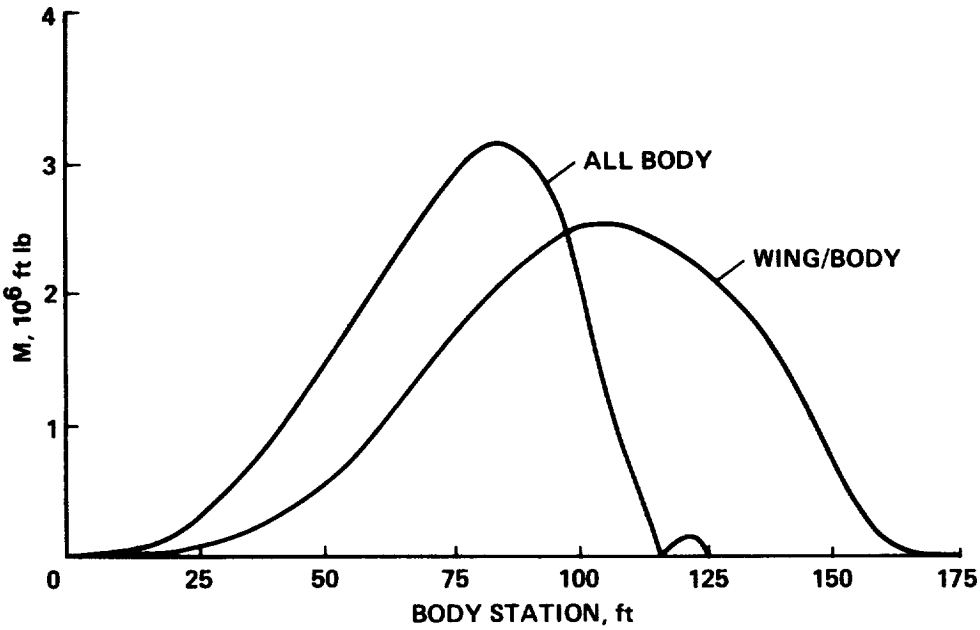

Figure 5.- Bending-moment distribution.

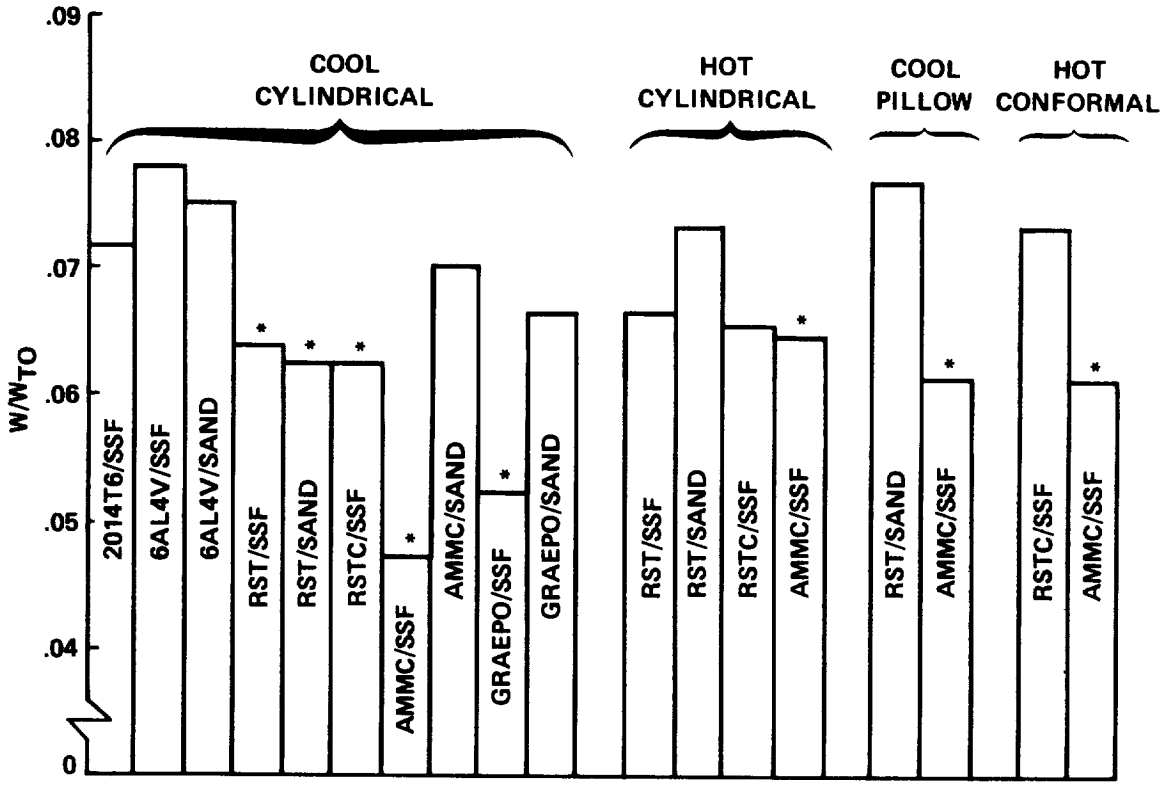

Figure 6.- A comparision of concepts.

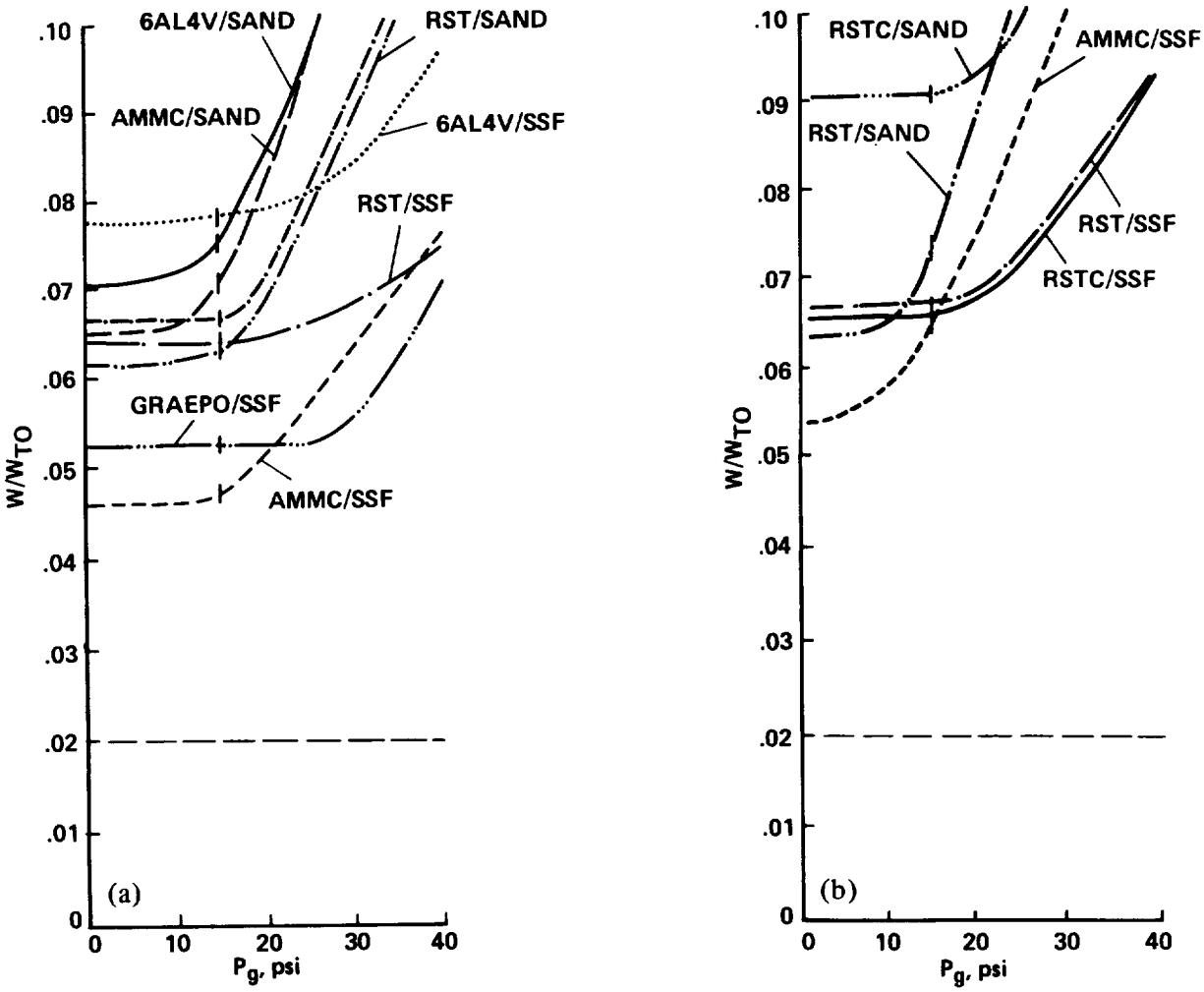

Figure 7.- The effect of gage pressure. (a) Cool cylindrical concept; (b) hot cylindrical concept.

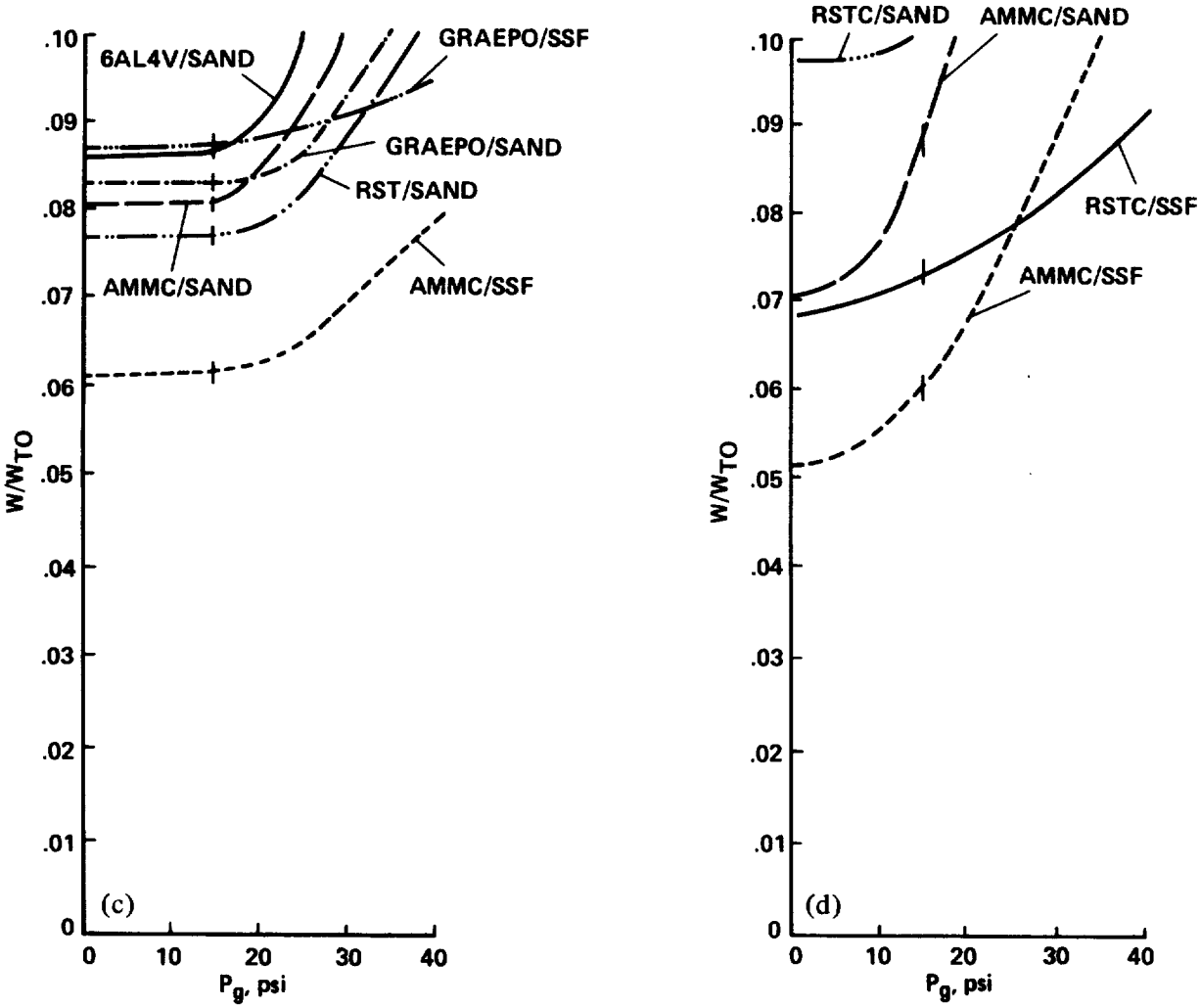

Figure 7.- Concluded. (c) Cool pillow concept; (d) hot conformal concept.

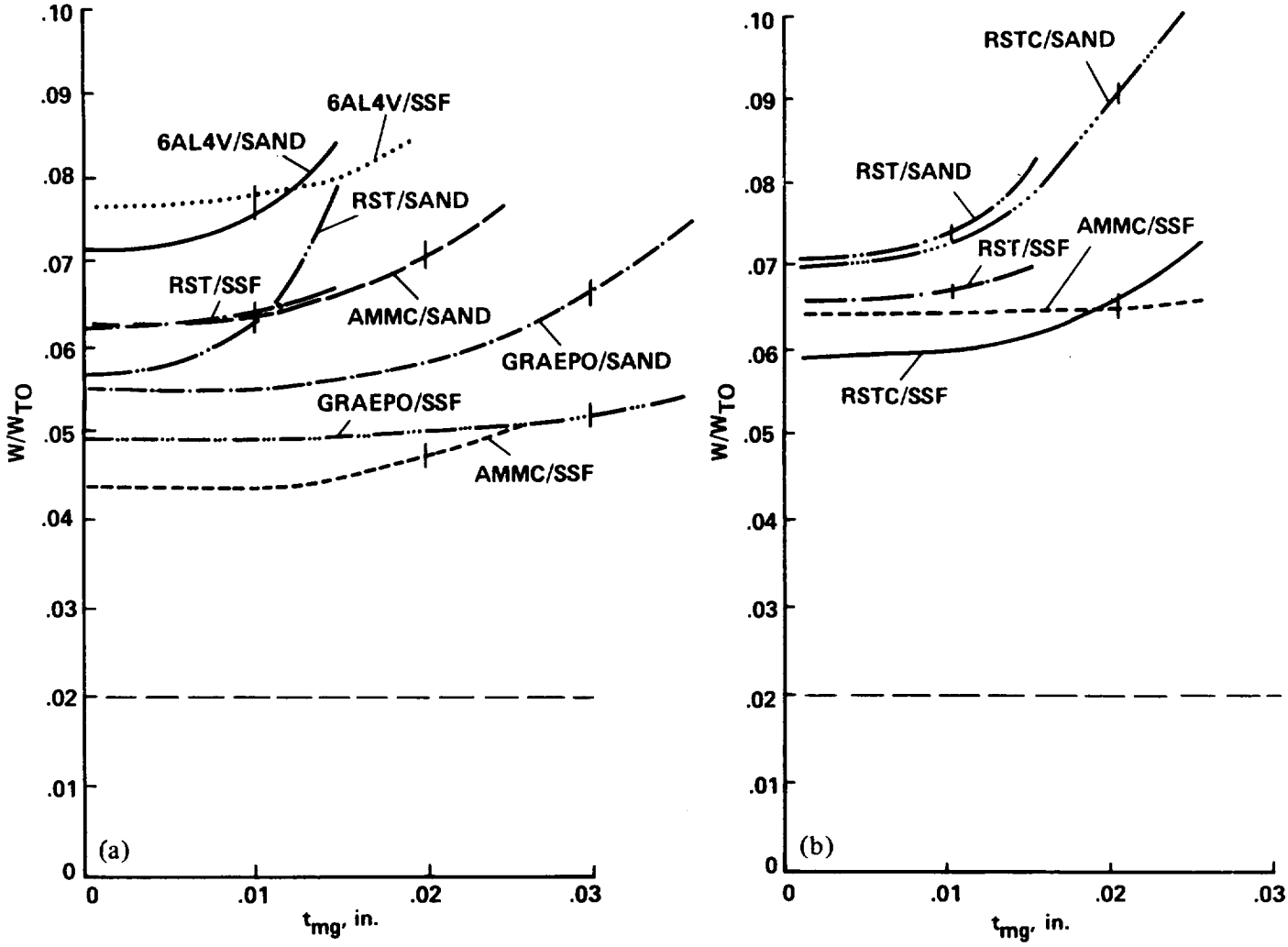

Figure 8.- The effect of minimum gage. (a) Cool cylindrical concept; (b) hot cylindrical concept.

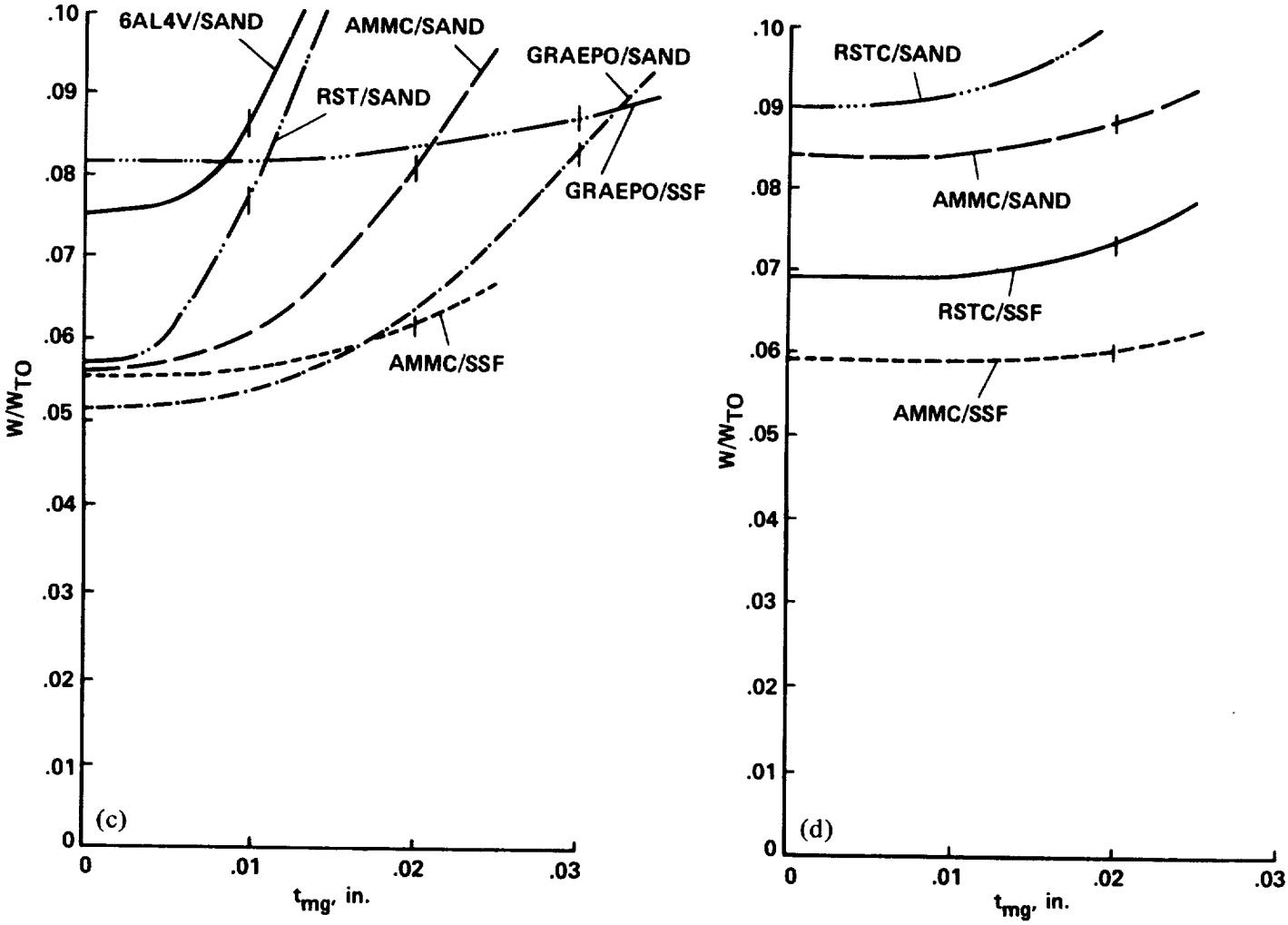

Figure 8.- Concluded. (c) Cool pillow concept; (d) hot conformal concept.

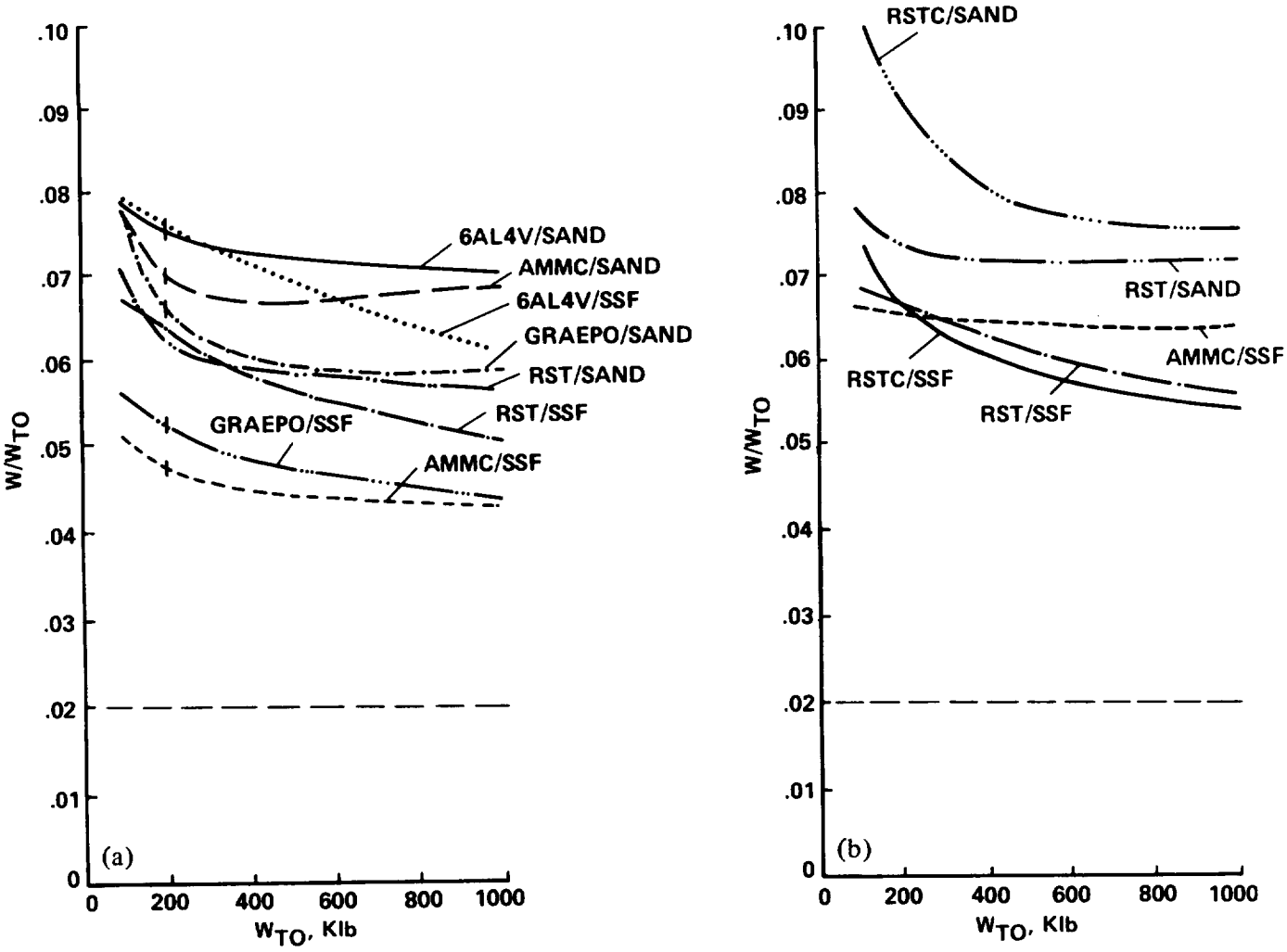

Figure 9.- The effect of gross take-off weight. (a) Cool cylindrical concept; (b) hot cylindrical concept.

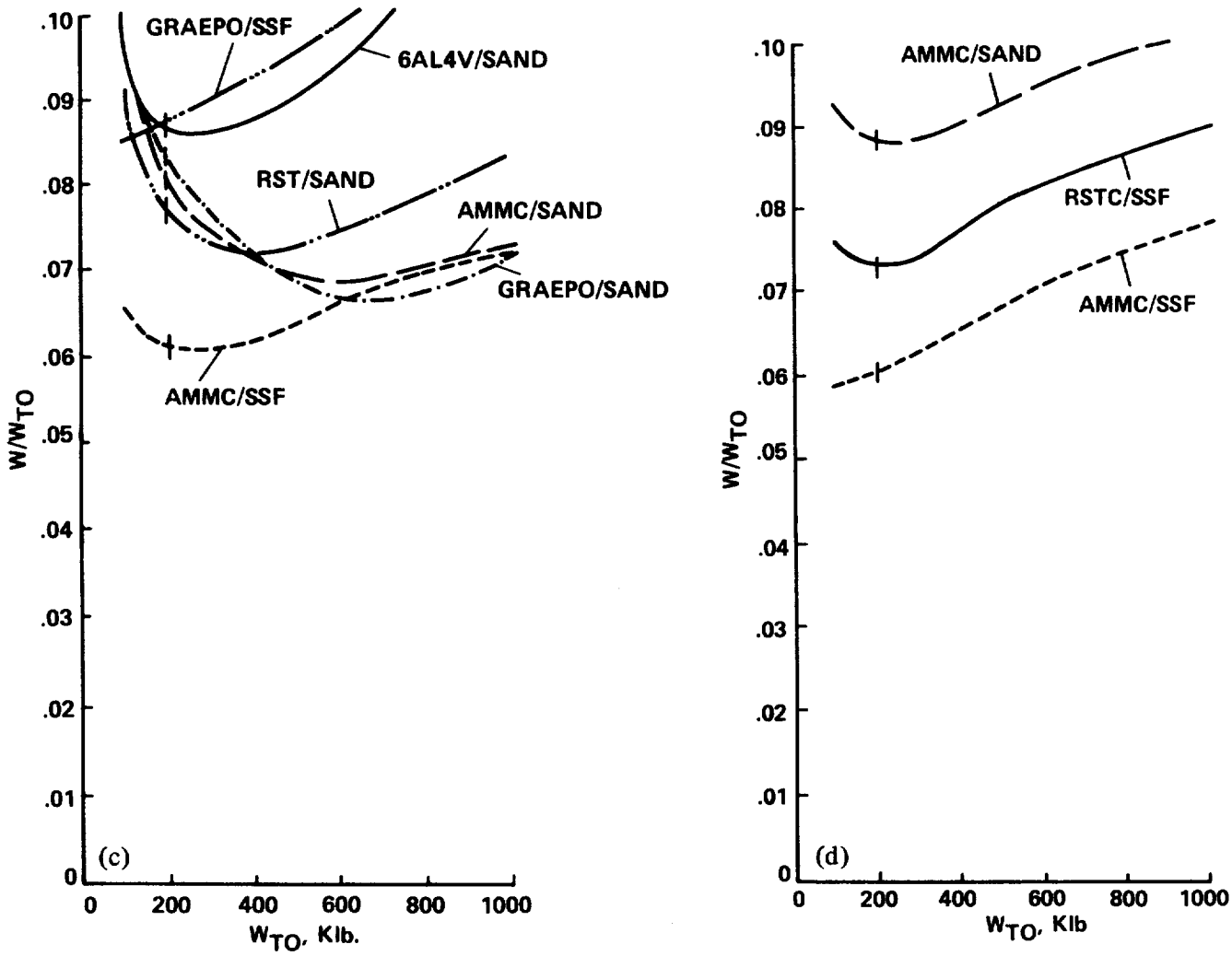

Figure 9.- Concluded. (c) Cool pillow concept; (d) hot conformal concept.

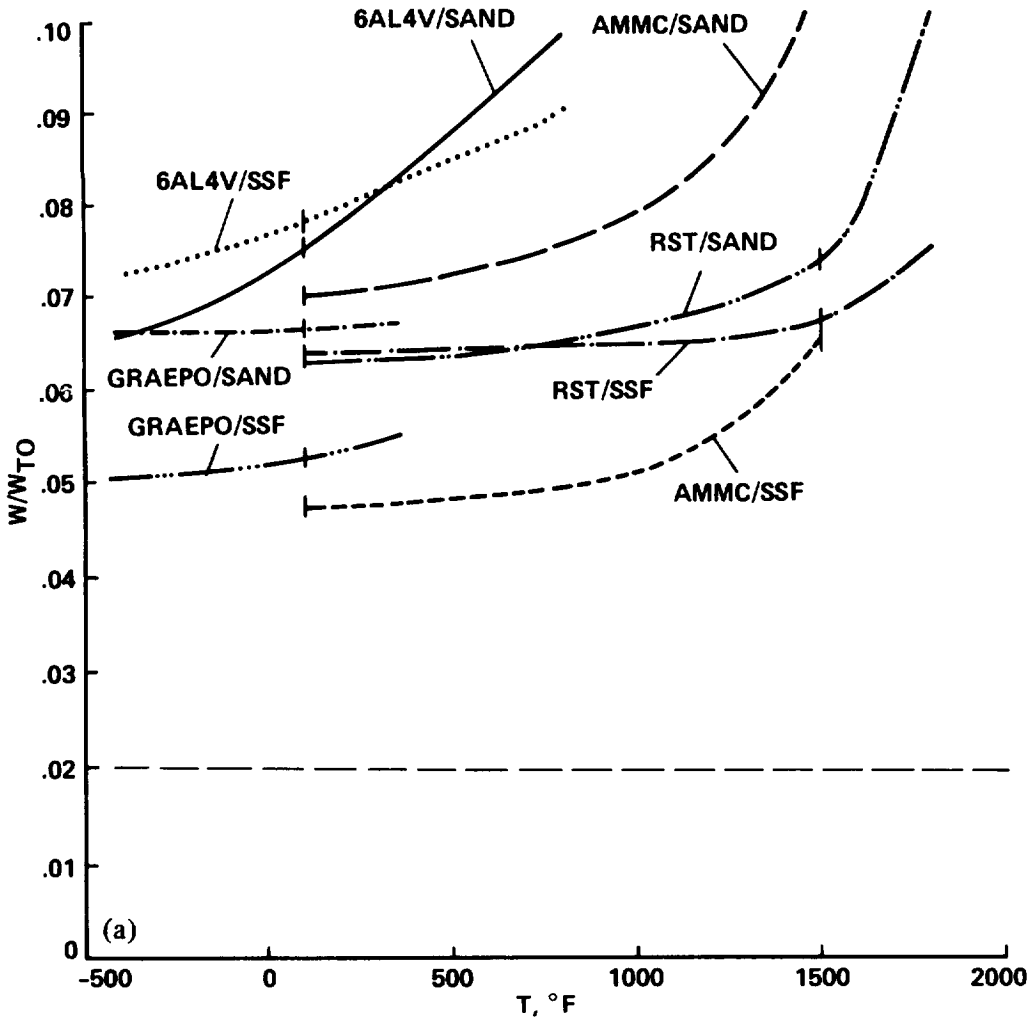

Figure 10.- The effect of structural temperature. (a) Hot and cool cylindrical concepts.

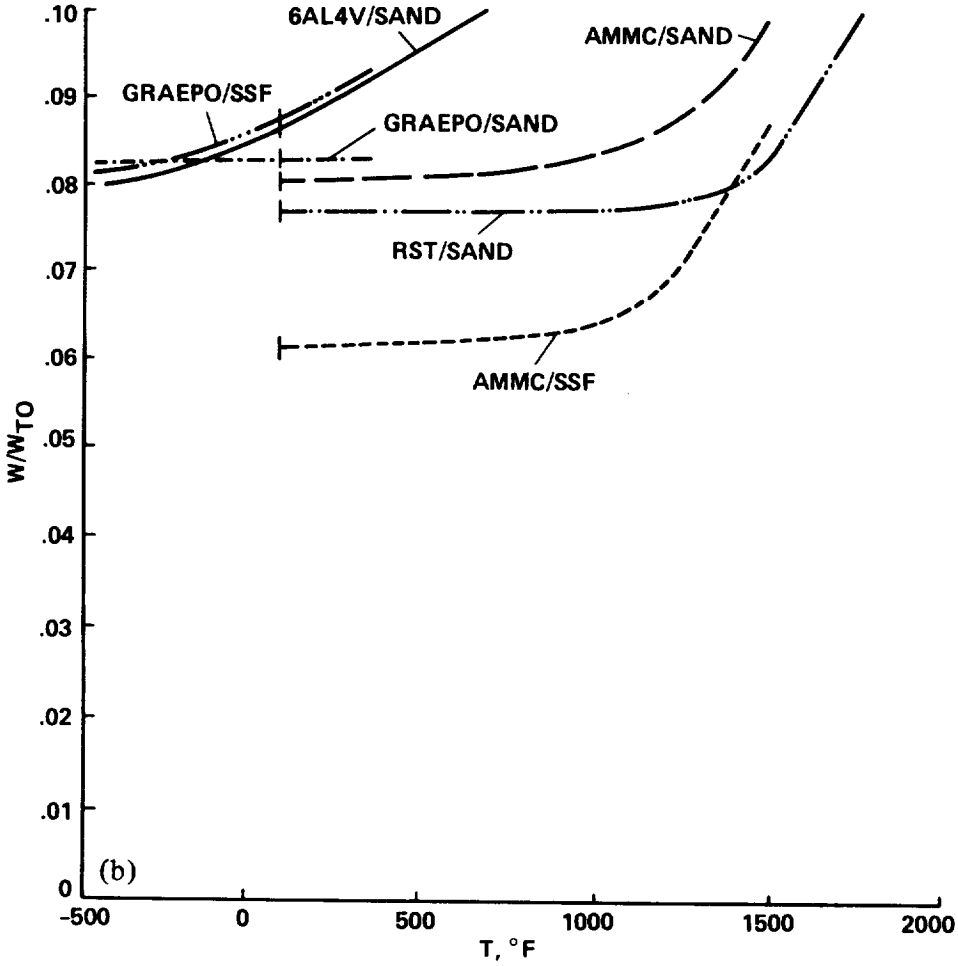

Figure 10.- Continued. (b) Cool pillow concept.

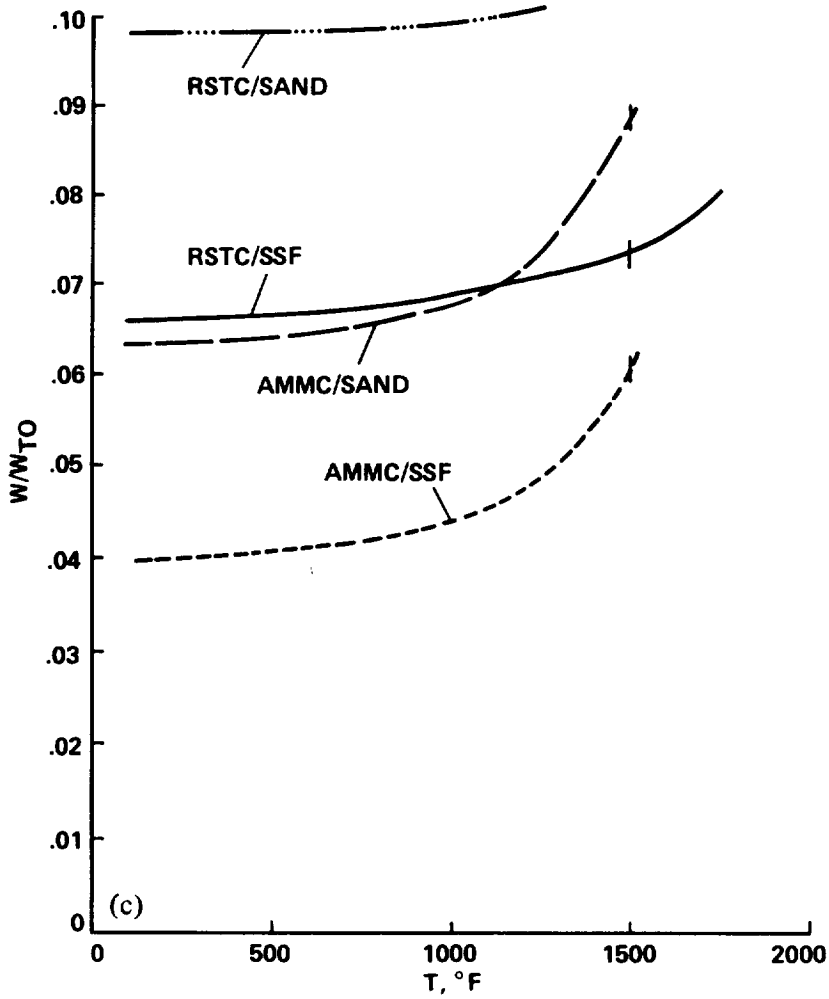

Figure 10.- Concluded. (c) Hot conformal concept.

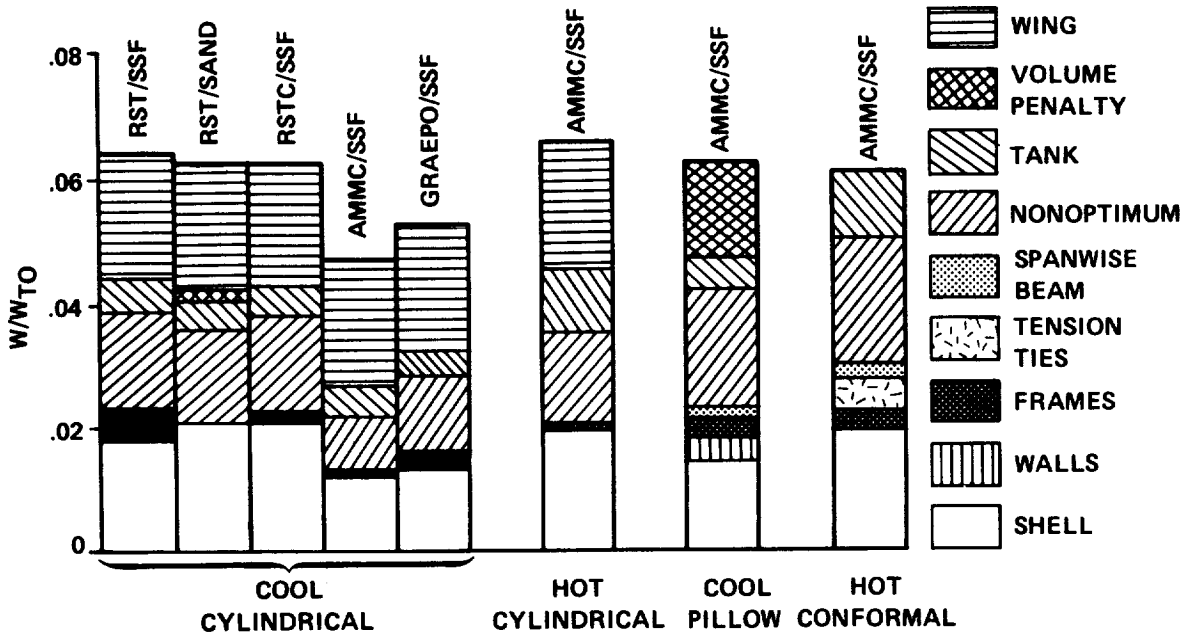

Figure 11.- Body structural weight breakdown.

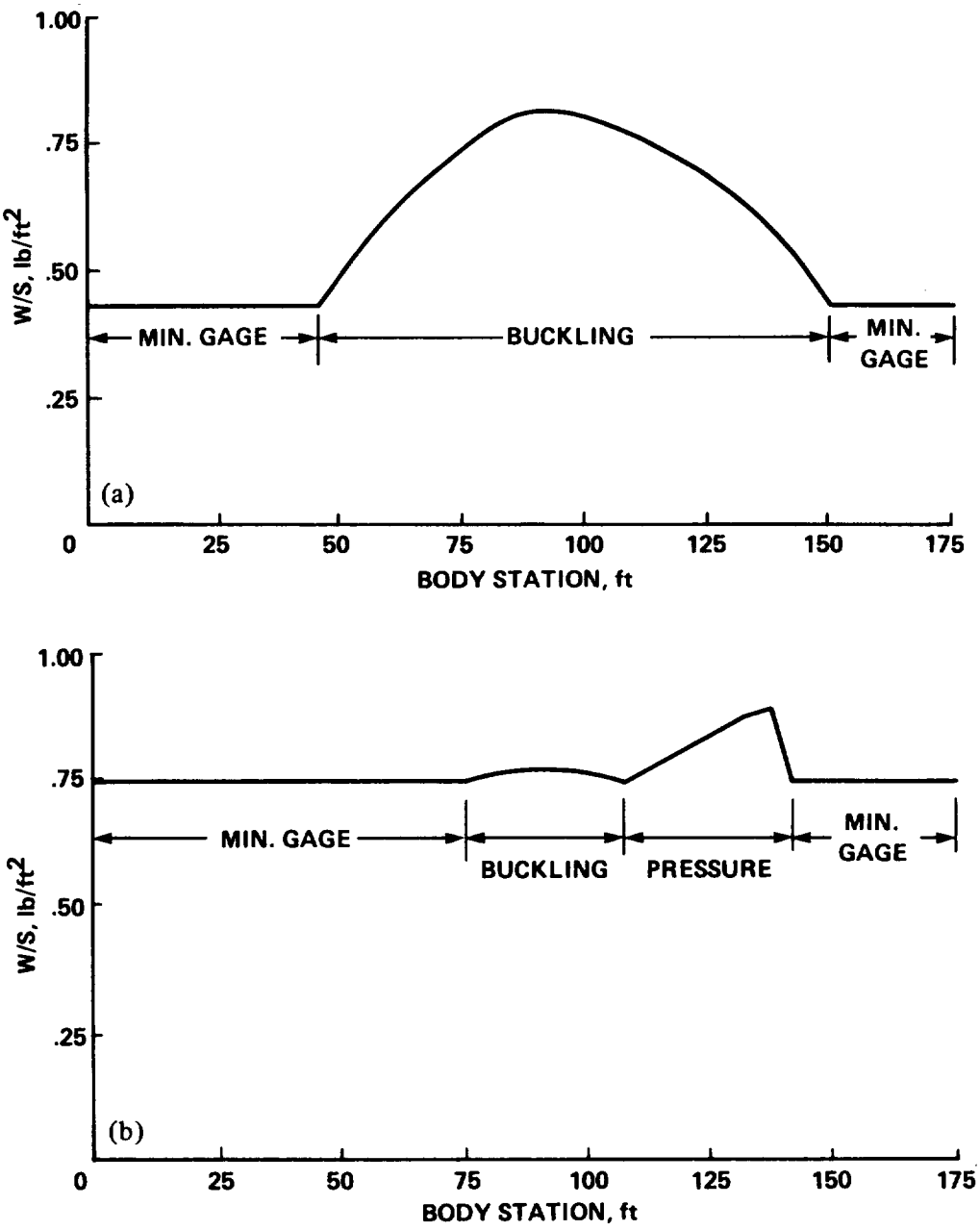

Figure 12.- Shell weight per unit surface area. (a) Cool cylindrical concept, RST/SSF; (b) cool cylindrical concept, RST/SAND.

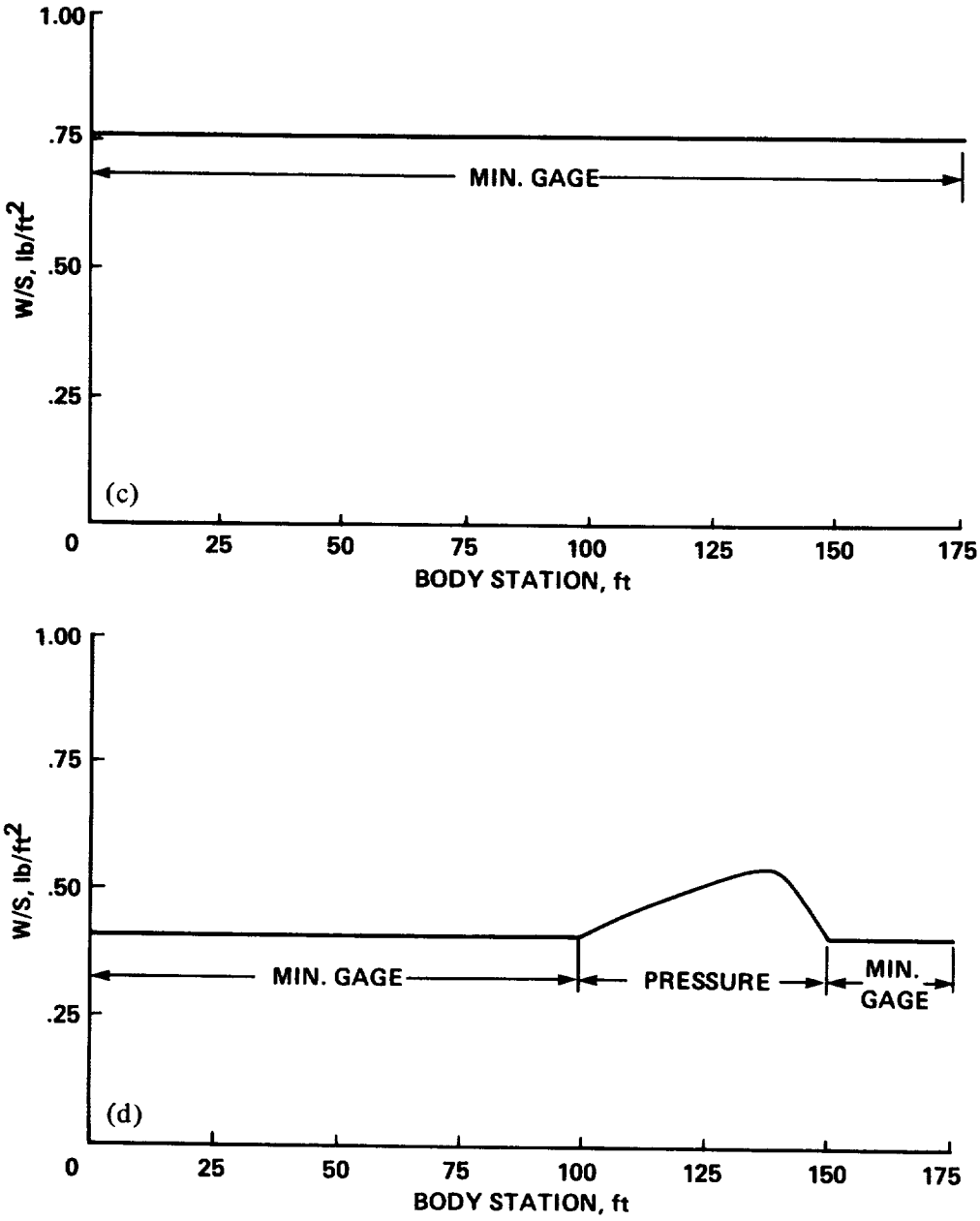

Figure 12.- Continued. (c) Cool cylindrical concept, RSTC/SSF; (d) cool cylindrical concept, AMMC/SSF.

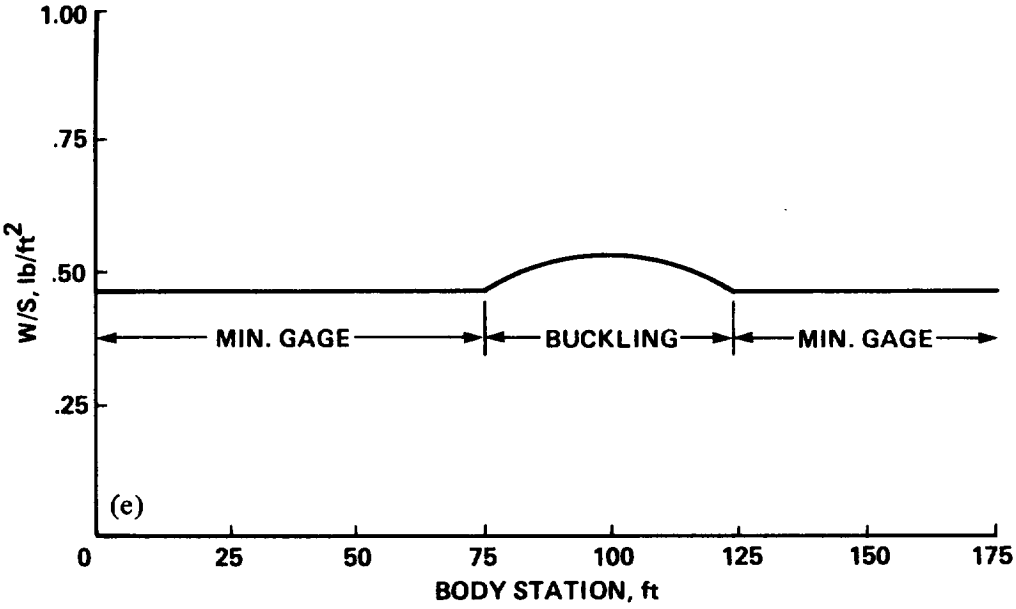

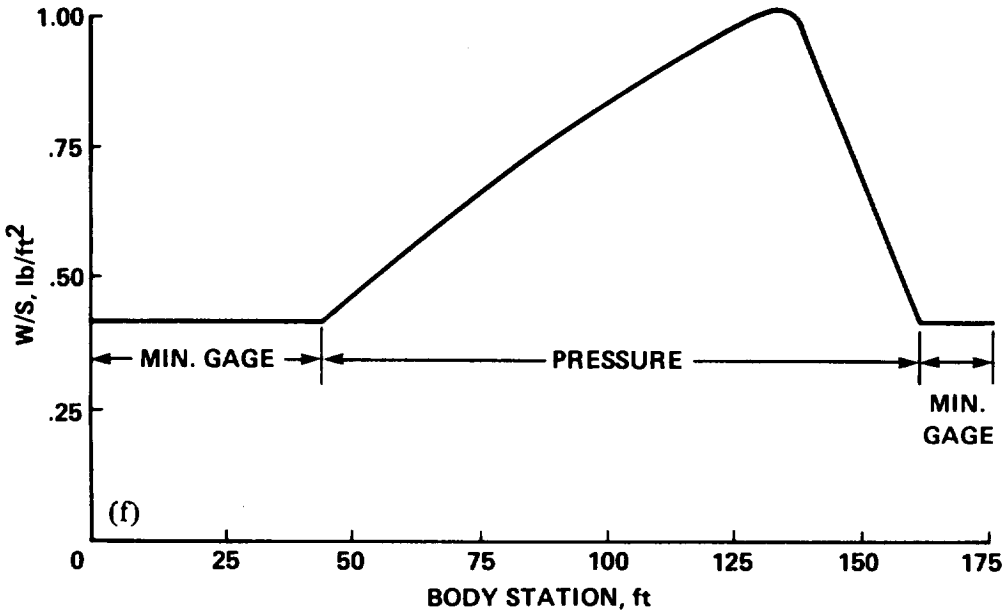

Figure 12.- Continued. (e) Cool cylindrical concept, GRAEPO/SSF; (f) hot cylindrical concept, AMMC/SSF.

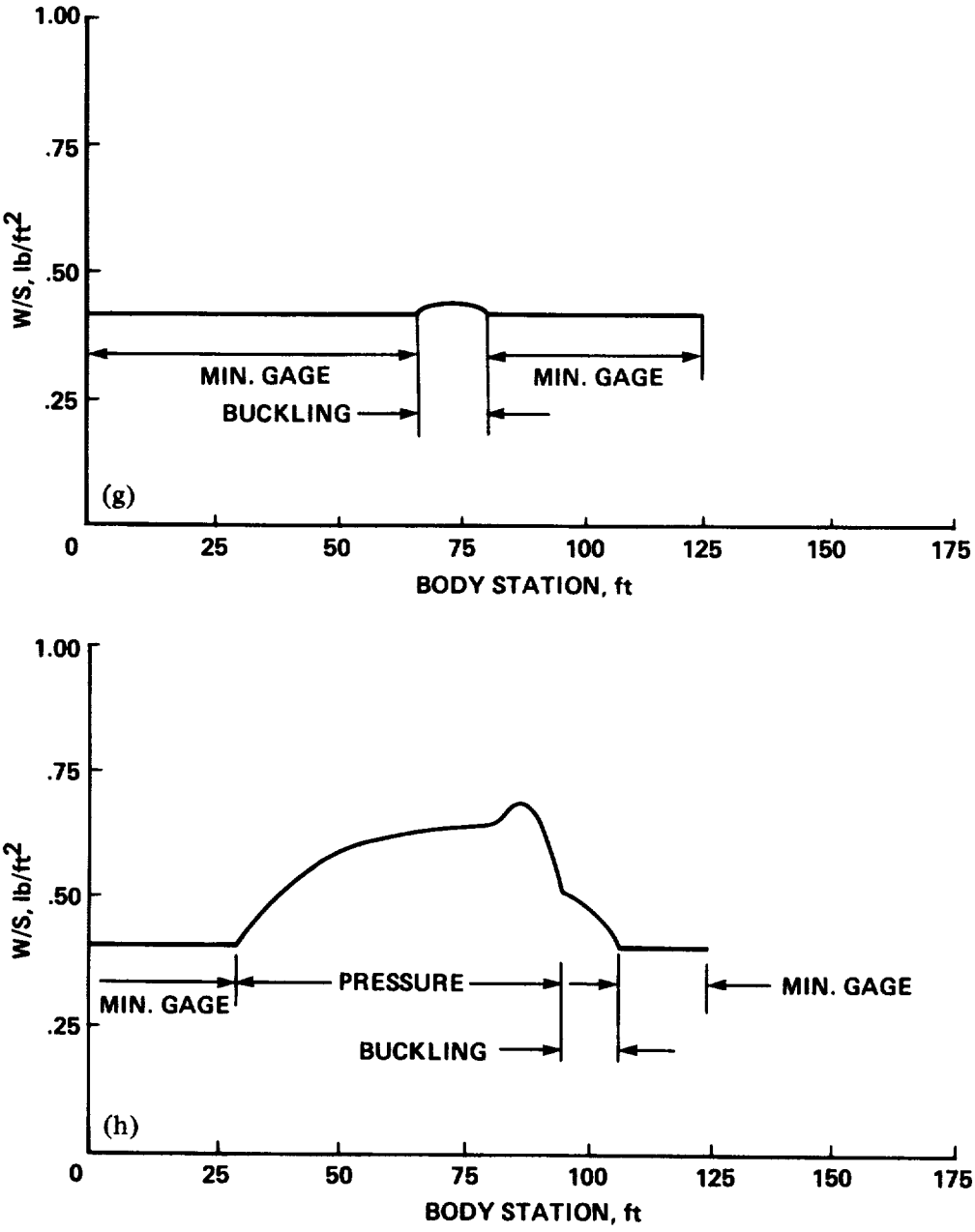

Figure 12.- Concluded. (g) Cool pillow concept, AMMC/SSF; (h) hot conformal concept, AMMC/SSF.

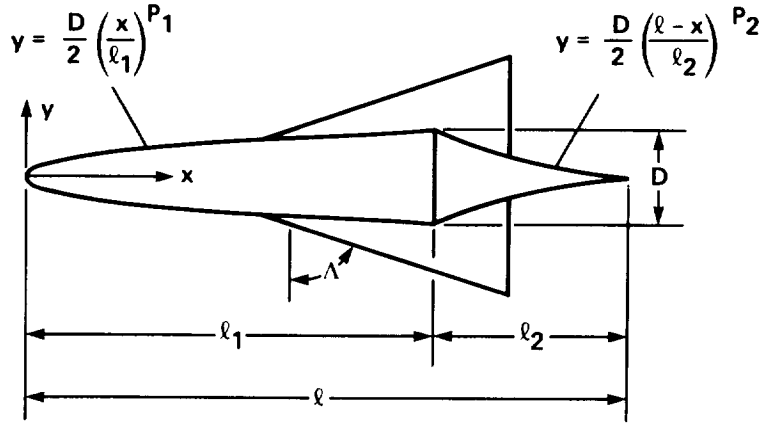

Figure A1.- The wing-body geometry.

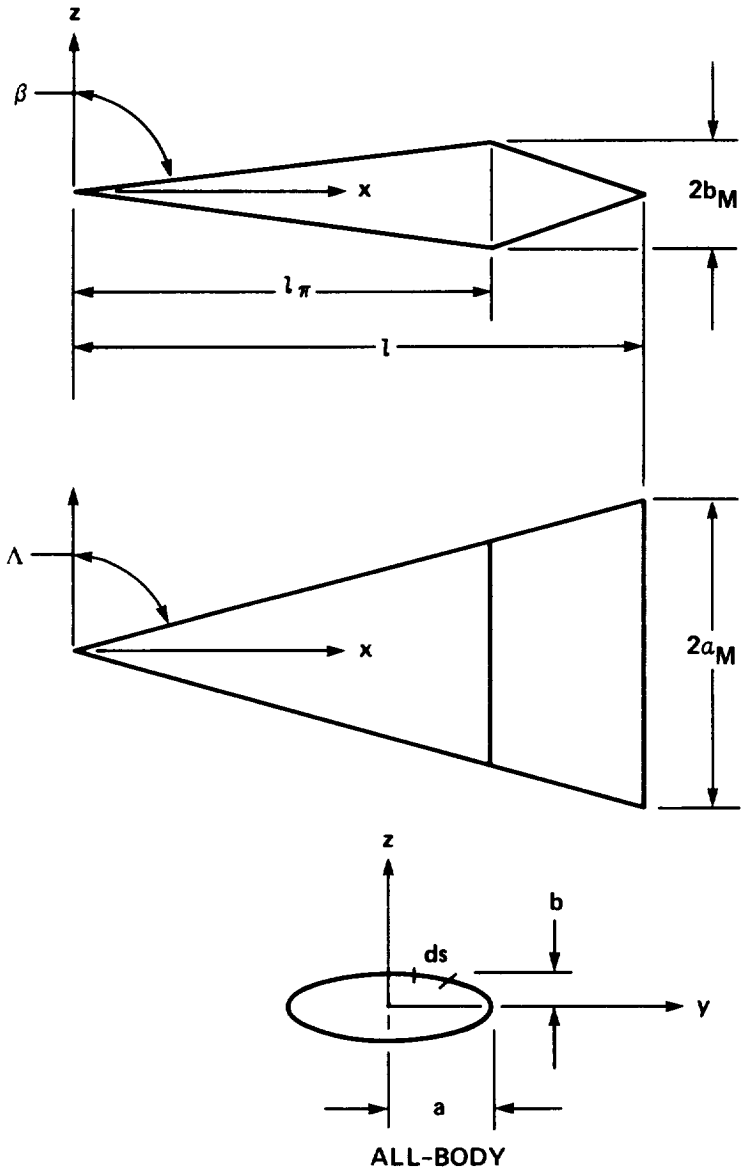

Figure A2.- The all-body geometry.

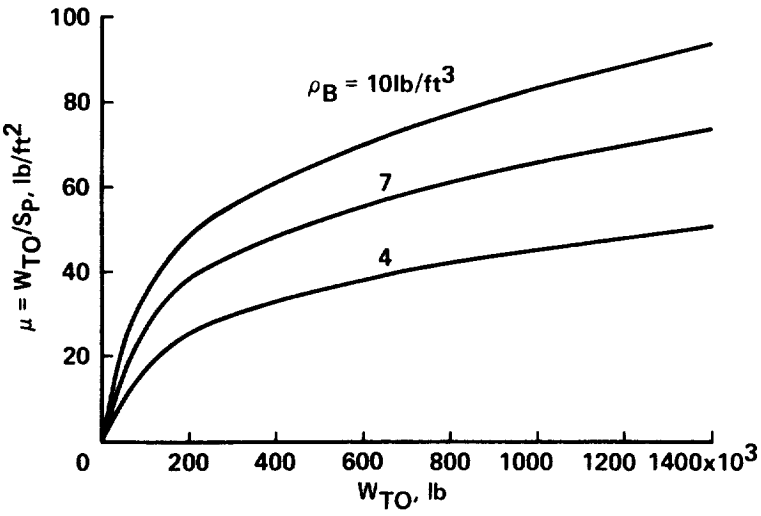

Figure A3.- Wing loading for the all-body configuration.

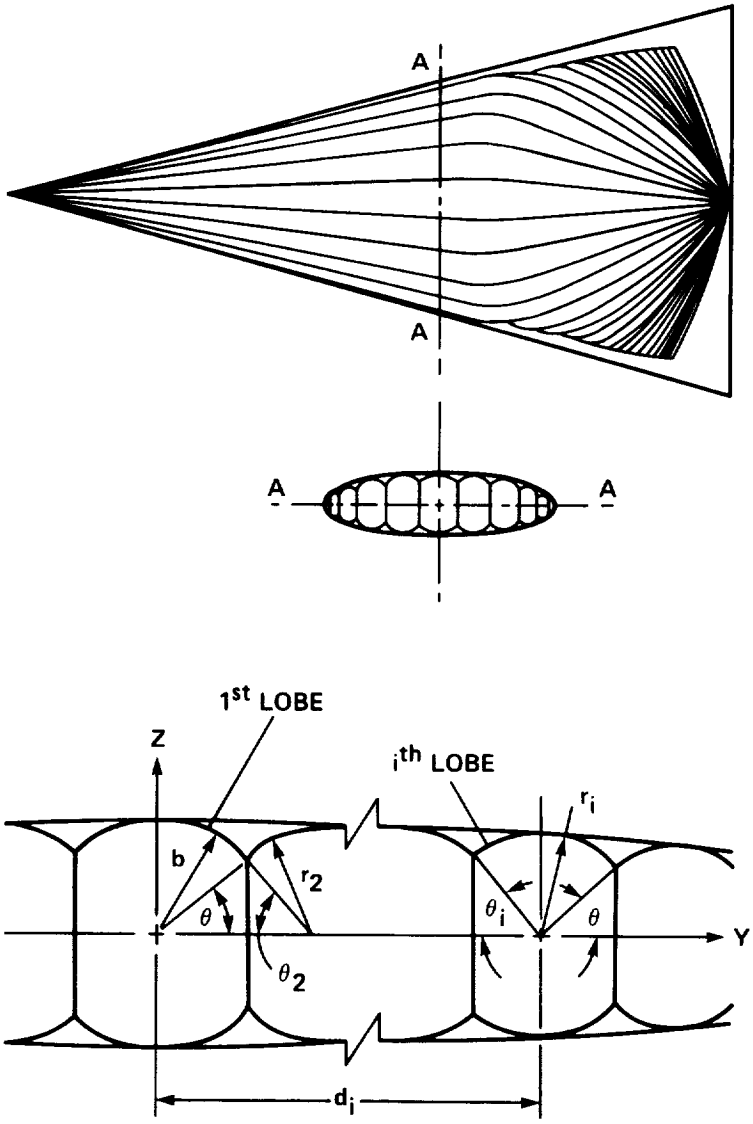

Figure A4.- The pillow tank geometry.

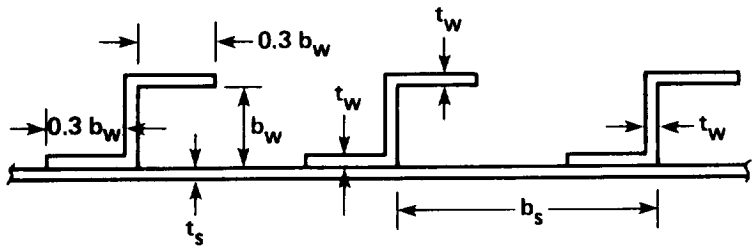

Figure B1.- The Z-stiffened shell geometry.

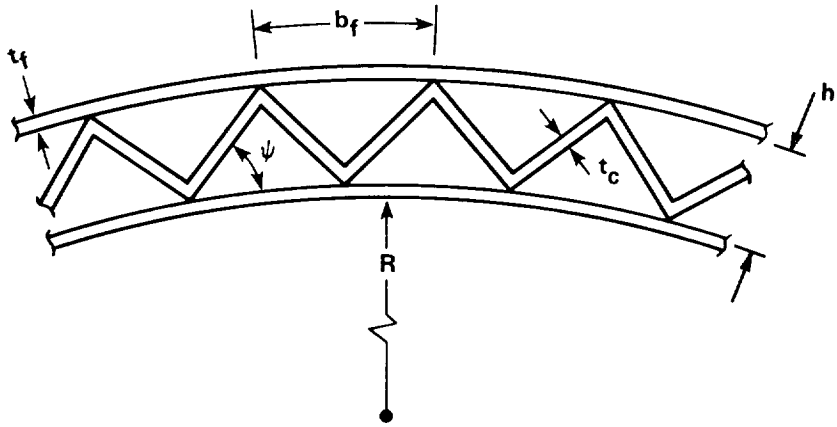

Figure B2.- The truss-core sandwich geometry.

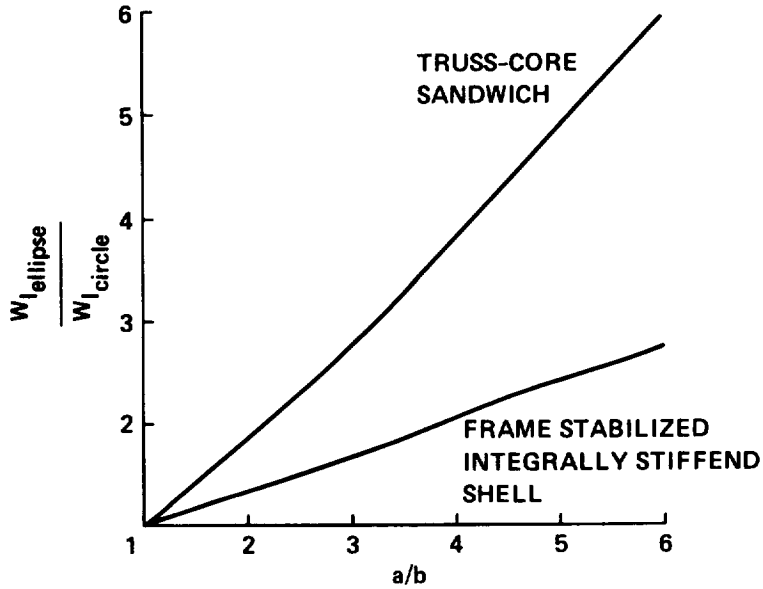

Figure B3.- A comparision of weights of unpressurized elliptic and circular shells.

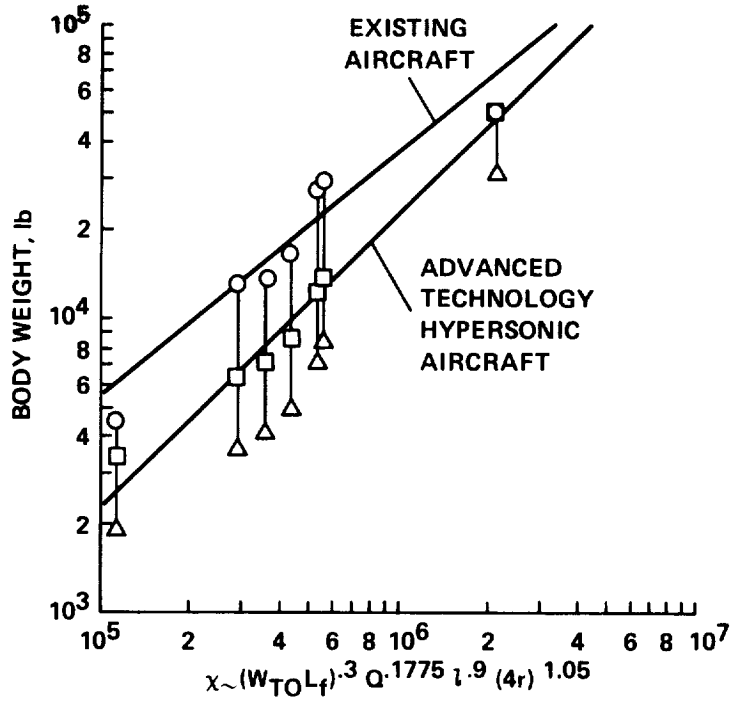

Figure B4.- Correlations and comparisons of body weight.

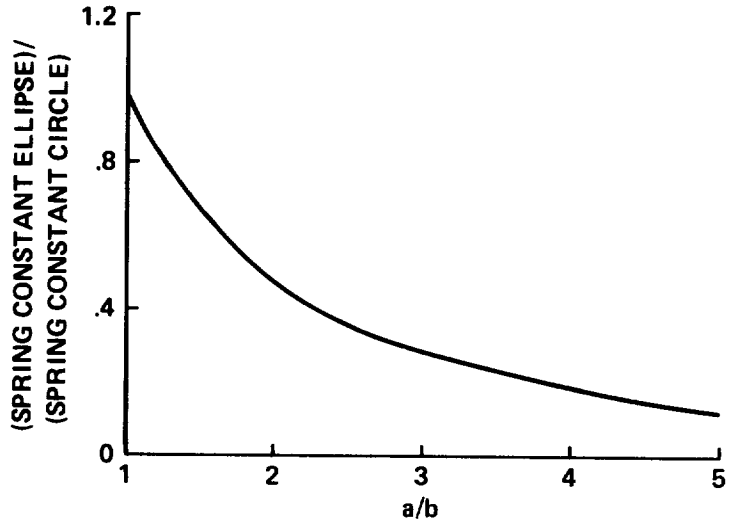

Figure C1.- A comparision of spring constants of elliptic and circular frames.

NASA National Aeronautics and Space Administration

Report Documentation Page

1. Report No.	2. Government Accession No.	3. Recipient's Catalog No.
NASA TM 101028		

4. Title and Subtitle	5. Report Date
Bodyweight of Hypersonic Aircraft: Part 1	October 1988
	6. Performing Organization Code

7. Author(s)	8. Performing Organization Report No.
Mark D. Ardema	A 88279
	10. Work Unit No. 763-01-61

9. Performing Organization Name and Address	11. Contract or Grant No.
Ames Research Center Moffett Field, CA 94035	
	13. Type of Report and Period Covered
12. Sponsoring Agency Name and Address	Technical Memorandum
National Aeronautics and Space Administration Washington, DC 20546	14. Sponsoring Agency Code

15. Supplementary Notes

Point of Contact: Mark D. Ardema, Ames Research Center, M/S 237-11
Moffett Field, CA 94035 (415) 694-6578 or FTS 464-6578

16. Abstract

The load-bearing body weight of wing-body and all-body hypersonic aircraft is estimated for a wide variety of structural materials and geometries. Variations of weight with key design and configuration parameters are presented and discussed. Both hot and cool structure approaches are considered in isotropic, organic composite, and metal matrix composite materials; structural shells are sandwich or skin-stringer. Conformal and pillow-tank designs are investigated for the all-body shape. The results identify the most promising hypersonic aircraft body-structure-design approaches and their weight trends. Geometric definition of vehicle shapes and structural analysis methods are presented in appendices.

17. Key Words (Suggested by Author(s))	18. Distribution Statement
Hypersonic aircraft Structural weight Aircraft design	[redacted] Unclassified-~~Unlimited~~ October 1990 Subject Category - 05

19. Security Classif. (of this report)	20. Security Classif. (of this page)	21. No. of pages	22. Price
Unclassified	Unclassified	62	A05

NASA FORM 1626 OCT 86

[redacted]